https://doi.org/10.5194/egusphere-2026-3700
Preprint. Discussion started: 24 July 2026

Towards Better Simulations of Liquid Water Path during Stratocumulus-to-Cumulus Transition: Insights from Gaussian Process Emulator, XGBoost and MAGIC Observations

Pratapaditya Ghosh[1], Xue Zheng[1], Hassan Beydoun[1], Peter Bogenschutz[1], and Yunyan Zhang[1]

[1]Lawrence Livermore National Laboratory, 7000 East Avenue, Livermore, CA, USA

Correspondence: Pratapaditya Ghosh (ghosh9@llnl.gov)

Abstract. Simulating Liquid Water Path (LWP) during stratocumulus-to-cumulus transition (SCT) remains challenging for storm-resolving models, with biases varying across cloud regimes. We use the storm-resolving DP-EAMxx model and a perturbed-parameter ensemble of three warm-rain microphysical parameters to investigate LWP biases during an SCT event observed in the MAGIC field campaign. Gaussian process emulators trained on observation-derived metrics of mean LWP bias and LWP decorrelation timescale bias are used to identify low-bias parameter combinations within the explored parameter space. While similar parameter constraints are obtained for the stratocumulus (Sc) and transition (Tr) phases, the low-bias parameter combinations for the cumulus (Cu) phase differ substantially, indicating requirement of a stronger reduction in autoconversion and accretion rates for a given prescribed droplet number concentration. Using an overlapping low-bias parameter set from the Sc and Tr phases, the mean LWP bias improves from -31 and -22 g m^{-2} to -1 and 3 g m^{-2} in the Sc and Tr phases, respectively, but degrades in the Cu phase. An independent XGBoost model with SHAP attribution, trained using DP-EAMxx-simulated process-level diagnostics and meteorological state, supports the emulator sensitivities: LWP bias in Sc is strongly associated with warm-rain microphysics, whereas dynamical, radiative, and thermodynamic influences become more prominent in Tr and Cu. These results show where a limited set of parameters is effective in improving model performance and where additional sources of uncertainty likely need to be considered across regimes. More broadly, we demonstrate a proof-of-concept observation-constrained framework for the diagnosis of storm-resolving model bias.

1 Introduction

Marine stratocumulus clouds play a key role in Earth's radiation budget by reflecting a significant amount of incoming solar radiation (Chen et al., 2000; Wood, 2012; Bretherton et al., 2004; Hartmann and Short, 1980). The stratocumulus cloud deck over the Northeast Pacific Ocean is one of the largest subtropical cloud decks (Mechoso et al., 2014; Wood et al., 2011). Overcast Stratocumulus cloud decks persist near the coast of California. However, as the trade winds advect them over continuously increasing sea-surface temperatures (SST) towards the equator, shallow broken Cumulus clouds become more prominent. This Stratocumulus-to-Cumulus transition (SCT) is associated with a reduction in cloud cover, liquid water path (LWP), and a weakening of the cloud radiative effects.

https://doi.org/10.5194/egusphere-2026-3700
Preprint. Discussion started: 24 July 2026

Two main theories have been proposed, based on observations and modeling, to explain the SCT. The 'Deepening-Warming-Decoupling' hypothesis proposes that warmer SSTs increase surface latent heat fluxes and deepen the marine boundary layer. This deepening leads to boundary-layer decoupling and the formation of cumulus clouds beneath the stratocumulus deck. The stratocumulus clouds eventually dissipate via cumulus-driven overshooting entrainment of dry free-tropospheric air (Bretherton, 1992; Bretherton and Wyant, 1997; Wyant et al., 1997; Sandu and Stevens, 2011). This SST-driven transition increases the role of surface forcing relative to cloud-top radiative cooling. Alternatively, the 'Precipitation-Drizzle-Feedback' theory proposes a relatively fast transition, where the drizzle in cumulus clouds is transported to stratocumulus clouds via updrafts, removing droplets (via collision-coalescence) and aerosols (via wet scavenging). This leads to a cleaner environment that favors larger drops, stronger precipitation, and accelerated LWP depletion, ultimately resulting in the breakdown of stratocumulus clouds (Yamaguchi et al., 2017; Wood et al., 2018; Diamond et al., 2022; Erfani et al., 2022). Because the relative importance of precipitation, entrainment, and boundary-layer coupling changes across the SCT, biases in simulated LWP are also likely to be regime dependent.

Simulating SCT remains a major challenge for atmospheric models (Eastman et al., 2021; Qu et al., 2014; Lin et al., 2014; Teixeira et al., 2011; Zuidema et al., 2016; Grosvenor and Carslaw, 2020). The modeled boundary-layer cloud fraction can be too low, and the transition too rapid (Zhang et al., 2024b; Jian et al., 2021; Bogenschutz et al., 2013). Biases are attributed to overly simplified subgrid-scale cloud parameterizations and the inability to resolve fine-scale processes such as warm-air entrainment across the cloud-top inversion (Schneider et al., 2017; Bretherton, 2015). With the rise of computationally intensive global storm-resolving models (Nowak et al., 2025; Caldwell et al., 2021; Stevens et al., 2019; Zhou et al., 2024; Peng et al., 2024), there is a growing opportunity to study mesoscale convection and associated radiative effects at high fidelity, with potentially better scale-aware microphysics and resolved km-scale processes. However, these high-resolution models still struggle with moderate to large biases in LWP and cloud fraction during SCT, leading to uncertainties in precipitation and cloud radiative effects (Bogenschutz et al., 2025; Makgoale and Sullivan, 2025). Additionally, the magnitude of model biases varies across different SCT stages. These biases likely reflect coupled uncertainties in warm-rain microphysics, cloud-top entrainment, boundary-layer structure, and environmental forcing, making it necessary to diagnose both the sensitivity and the regime dependence of LWP bias.

Machine learning (ML)-based algorithms are increasingly used to understand (and potentially improve) microphysics, radiation, turbulence, and aerosol cloud interactions in atmospheric models (Gettelman et al., 2021; Li et al., 2019; Ukkonen, 2022; Fuchs et al., 2024; Perkins et al., 2024; Zhang et al., 2024a; Prévost et al., 2026; Shin and Howland, 2026). With the availability of greater computational resources, atmospheric models are becoming more physically sophisticated but also more complex and subject to larger parametric uncertainties. Surrogate models and perturbed parameter ensembles (PPEs) are emerging as important tools to increase model reliability (Carslaw et al., 2026). Recent work by Erfani et al. (2025) utilized principal component analysis and large-eddy simulations (LES) to characterize a library of Lagrangian trajectories and investigate how aerosol perturbations influence cloud breakup and radiative effects during the SCT. Sansom et al. (2026) used a PPE of idealized LES simulations and Gaussian process emulators to show how aerosol concentration and environmental factors jointly influence the SCT. While these approaches are valuable, fewer studies have integrated surface-based observations di-

https://doi.org/10.5194/egusphere-2026-3700
Preprint. Discussion started: 24 July 2026

rectly into such frameworks, rather than relying primarily on passive remote-sensing retrievals with larger uncertainties. Zhang et al. (2026) recently combined ML, Atmospheric Radiation Measurement (ARM) observations, and storm-resolving model simulations to address parametric uncertainties in turbulence parameterizations for clear-sky convective boundary layers and continental shallow cumulus regimes. Together, these studies highlight the importance of observation-constrained and interpretable ML approaches, but a similar framework has not yet been widely applied to diagnose regime-dependent LWP biases across the SCT in storm-resolving models.

In this study, we combine observations from an ARM field campaign with two complementary ML approaches to diagnose regime-dependent LWP bias in a storm-resolving model during a SCT event. We focus on a set of three warm-rain microphysical parameters to provide an interpretable proof-of-concept assessment of parametric sensitivity. Our objectives are to: (1) quantify how LWP bias depends on these parameters across the stratocumulus, transition, and cumulus phases using surrogate emulators; (2) assess whether a shared low-bias parameter region exists across different phases when different constraints are applied; and (3) use an independent explainable ML analysis to diagnose which modeled physical processes are strongly associated with LWP bias in each regime. Our aim is to identify low-bias parameter combinations within the explored warm-rain parameter space, and to distinguish where bias reduction is achievable through tuning of these parameters and where additional sources of uncertainty likely need to be considered. Section 2 describes the model configuration, Sections 3 and 4 describe the methodology, and Section 5 presents the results.

2 Storm-Resolving Model Configuration

The doubly periodic configuration of the Simple Cloud-Resolving E3SM Atmosphere Model (DP-SCREAM) (Bogenschutz et al., 2023) has recently been evaluated against several ARM observations (Bogenschutz et al., 2025). In this work, we use the C++ codebase (DP-EAMxx) of the DP-SCREAM (Bogenschutz et al., 2025; Donahue et al., 2024), implemented using the Kokkos library (Trott et al., 2022). DP-EAMxx (DP hereafter) enables convection-permitting simulations within the E3SM framework by applying periodic lateral boundary conditions over a finite domain. It is designed for controlled experiments of cloud systems under prescribed large-scale forcings while retaining the full global SCREAM physics suite, including turbulence, shallow convection, and microphysics parameterizations. This framework provides a computationally efficient platform for process-level evaluation, and has demonstrated skill in reproducing observed cloud behavior and diagnosing structural model biases. The dynamics grid spacing in our simulation is $\sim$ 3.2 km, with dynamics time step of 10 s and a physics time step of 120 s. Aerosols are prescribed using the Simple Prescribed Aerosol (SPA) scheme (Donahue et al., 2024). Fluid dynamics is handled by the non-hydrostatic High Order Method Modeling Environment (HOMME-NH) (Bertagna et al., 2020; Taylor et al., 2020; Dennis et al., 2005, 2012). Clouds and turbulence are parameterized using the Simplified Higher Order Closure (SHOC) scheme (Bogenschutz and Krueger, 2013), while microphysical processes are represented using the Predicted Particle Properties (P3) scheme, a two-moment bulk warm-phase microphysics formulation following Morrison and Milbrandt (2015).

https://doi.org/10.5194/egusphere-2026-3700
Preprint. Discussion started: 24 July 2026

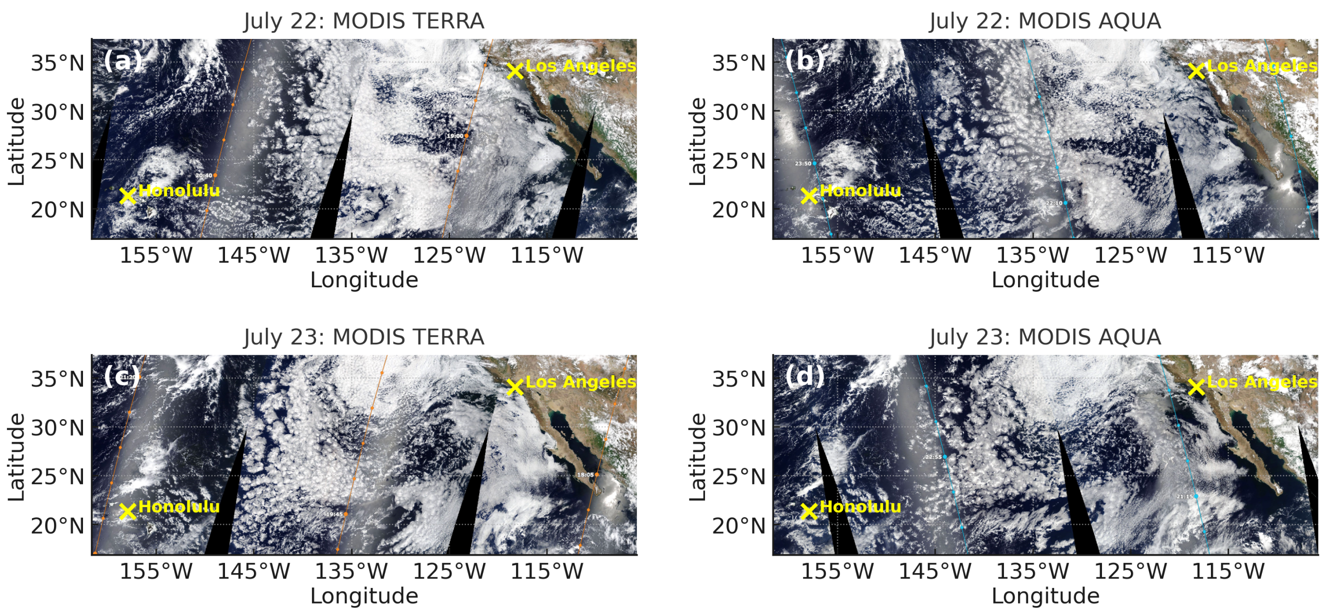

Figure 1. MODIS true-color imagery showing the stratocumulus-to-cumulus transition over the eastern Pacific near Hawaii and California on July 22-23, 2013. (a) Terra, July 22 (20:00 UTC; 13:00 PDT); (b) Aqua, July 22 (22:00 UTC; 15:00 PDT); (c) Terra, July 23 (20:00 UTC; 13:00 PDT); (d) Aqua, July 23 (22:00 UTC; 15:00 PDT). Yellow X markers indicate the locations of Honolulu and Los Angeles. The ship track followed the route from Los Angeles to Honolulu.

This study focuses on one SCT event observed during leg 15A of the Marine ARM GPCI Investigation of Clouds (MAGIC) field campaign (Zhou et al., 2015). This leg spanned 21-24 July 2013, when the Horizon Spirit cargo ship traveled from Los Angeles (LA) to Honolulu in the Pacific Ocean. This event has been extensively studied with different high-resolution models, including LES, single-column models, and storm-resolving models (Zheng et al., 2020; Bogenschutz et al., 2025; McGibbon and Bretherton, 2017). Figure 1 shows the SCT on July 22-23 using the MODIS true-color imagery over the eastern Pacific near Hawaii and California. We observe a gradual transition from overcast stratocumulus clouds (near the California coast) to broken cumulus clouds (near Hawaii). The entire SCT event comprises three phases. Until 20:00 UTC on July 22 (38 hours from model initialization), during the Stratocumulus Phase (ScP), the cloud fraction remains high, with gradually decreasing relative humidity (RH) and increasing planetary boundary layer height (PBLH) (See Figure 3 right panel of Zheng et al. 2020). This phase is also described by Ghate et al. (2019). From hour 38 to 60, i.e. 18:00 UTC on July 23, the RH and PBLH gradually increase, marking the Transition Phase (TrP). Beyond hour 60, the cloud fraction is much lower in the Cumulus Phase (CuP). The cloud evolution of the default DP simulation (Supplement Figure S1) in most of the DP simulations conducted in this study follow the observed SCT evolution (Supplement Figure S2), supporting the robustness of this regime classification.

To understand the model performance, we use the observations of LWP, derived from a three-channel microwave radiometer and post-processed with an optimal estimation scheme, reducing the observational uncertainty to between 7 and

https://doi.org/10.5194/egusphere-2026-3700
Preprint. Discussion started: 24 July 2026

15 gm^{-2} (Ghate and Cadeddu, 2019; Cadeddu et al., 2013). The post-processed observations of LWP used here are 2-minute averages. The default DP simulation generally captures SCT but systematically underestimates LWP during the Stratocumulus Phase (details in Section 5.1). This underestimation of stratocumulus LWP, along with an overestimation of surface precipitation rate, are previously reported in Bogenschutz et al. (2025).

3 Perturbed Parameter Ensembles (PPE)

Among all cloud-controlling factors, this study focuses on the parameterized microphysical processes that directly regulate LWP and precipitation: cloud droplet concentration, autoconversion, and accretion. Together, they determine the precipitation efficiency and, consequently, the rate at which liquid water is removed from the cloud layer. The cloud droplet number concentrations (N_c) at the end of a model time step are calculated as:

$$N_c = \max(N_{c,preact}, C_{ccn}(N_{ccn} \times CF)^m) \quad (1)$$

where $N_{c,preact}$ is the model droplet concentrations before the empirical activation parameterization is used, N_{ccn} is the prescribed cloud condensation nuclei (CCN) concentration at 0.1% supersaturation, CF is the liquid cloud fraction in the grid box, and C_{ccn}, m are empirical constants. Hence, apart from advection, sedimentation, and different microphysical processes (which affect $N_{c,preact}$), N_c can only be reduced if the cloud completely evaporates in the grid box. This ratcheting mechanism (Stevens et al., 1996) is popular in other models (Lohmann, 2002; Gordon et al., 2020) and may lead to overestimation of N_c in km-scale models (Ghosh et al., 2025). C_{ccn} and m were attempted to be tuned in different versions of the development model. For example, these parameters in the recent EAMxx code branch are set to 2000, and 0.55 respectively following Mahfouz et al. (2025). Here, in our simulations, we set m to 1.0 for simplicity, same as Bogenschutz et al. (2025). The autoconversion and accretion rates are parameterized following Khairoutdinov and Kogan (2000), as shown in Equations 2 and 3.

$$P_{auto} = C_{auto}\,(q_c - q_{c0})^{\alpha} N_c^{-\beta} \quad (2)$$

$$P_{accr} = C_{accr}\, q_c^{\gamma}\, q_r^{\delta} \quad (3)$$

Here,

- q_c : cloud water mixing ratio
- q_r : rain water mixing ratio
- N_c : cloud droplet number concentration
- q_{c0} : threshold cloud water mixing ratio, set to zero in our simulations
- P_{auto} : autoconversion rate (q_c to q_r)

https://doi.org/10.5194/egusphere-2026-3700
Preprint. Discussion started: 24 July 2026

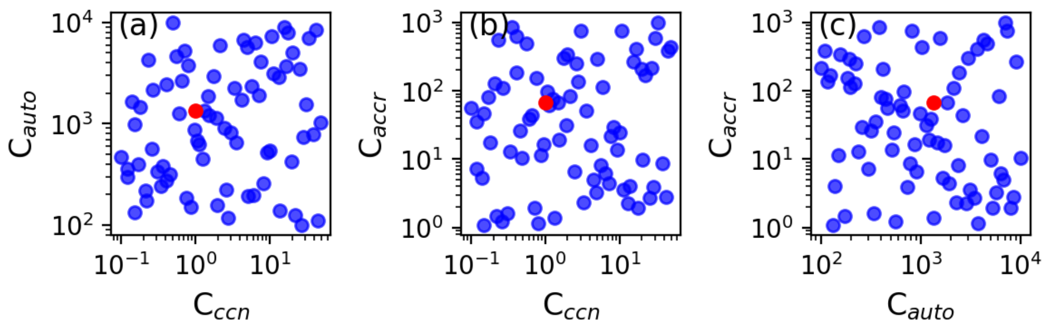

Figure 2. Scatter plots of the 75 parameter sets generated using Latin Hypercube Sampling (LHS), showing the pairwise relationships between (a) C_{ccn} and C_{auto}, (b) C_{ccn} and C_{accr}, and (c) C_{auto} and C_{accr}. The red dots indicate the default values of C_{ccn}, C_{auto}, and C_{accr}.

- P_{accr} : accretion rate (collection of q_c by q_r)
- C_{auto}, C_{accr}: empirical constants, set to 1350 and 67, respectively, in the default simulation
- α, β, γ, δ : scheme exponents from Khairoutdinov and Kogan (2000); often re-calibrated in different models (Xie et al., 2025, for example); in our simulations, we set $\alpha = 2.47, \beta = 1.79, \gamma = \delta = 1.15$

We perturb only one linear coefficient parameter for each process in P3: C_{ccn}, C_{auto}, and C_{accr}. This reduced parameter set is intended to provide a transparent proof-of-concept simple diagnosis, rather than an exhaustive sampling of all microphysical and boundary-layer uncertainties. These parameters are uncertain due to limited observational constraints and process complexity, yet they exert strong control over cloud microphysical evolution and, consequently, over LWP and precipitation. We vary these parameters in the ranges $[0.1, 50]$, $[10^2, 10^4]$, and $[1, 10^3]$ using Latin hypercube sampling (M. D. Mckay and Conover, 2000; Helton and Davis, 2003) in log space to generate a 75 member perturbed parameter ensemble (PPE) besides the default simulation. Figure 2 shows the combination of all three parameters for the PPE. The choice of the number of ensemble members typically depends on the number of input parameters. For instance, 250 ensemble members for 25 parameters by (Nugent et al., 2026), 250 members for 45 parameters by (Zhu et al., 2025), 221 members for 37 parameters by (Regayre et al., 2023), 121 members for 12 parameters by (Sanchez et al., 2026) and more recently, 34 members for 6 parameters by (Sansom et al., 2026). Based on these studies, our use of 76 members (75+1 Default) for 3 parameters appears to be both logical and sufficient. For each simulation, we use a 6 hour model spin up.

4 Machine Learning Models

We use two complementary ML approaches to (a) address microphysical parametric uncertainty by using surrogate emulators and to (b) understand the sensitivity of DP-simulated LWP bias to different controlling factors.

https://doi.org/10.5194/egusphere-2026-3700
Preprint. Discussion started: 24 July 2026

4.1 Gaussian Process Emulators (GPE) as Surrogate Models

Gaussian Processes (GPs) have been widely used for emulation and uncertainty quantification (Rasmussen and Williams, 2006; O'Hagan, 2006). A GP defines a distribution over functions and uses observed data to update this distribution, producing both a predictive mean (expected output) and a predictive variance (uncertainty estimate). This makes GPs particularly suitable for problems with limited training data, where quantifying uncertainty is as important as accurate prediction. Unlike tree-based ensemble methods, GPs do not require specifying a fixed model form; instead, they rely on kernel functions to encode smoothness, correlation, and other structural assumptions about the input–output relationship (see Supplement Text S1 for more details). We group the data into three cloud regimes : ScP, TrP, and CuP. Using the three microphysical parameters $(C_{ccn}, C_{auto}, C_{accr})$ as input, we trained two different types of GP emulators (GPE).

4.1.1 Emulator (a): Time-Averaged Domain-Mean $\mathrm{LWPB_{DP}}$

This GPE is specifically designed to predict the time-averaged DP-Simulated LWP Bias ($\mathrm{LWPB_{DP}}$). Using LWP observations from the MAGIC field campaign, we define the bias as: $\mathrm{LWPB_{DP}} = \mathrm{LWP_{DP}} - \mathrm{LWP_{obs}}$. The GPE is then trained on the mean of this value over the duration of each specific SCT phase. The 7-15 g m^{-2} uncertainty was reported for observations at much higher frequency compared to ~ 30 hours average we use while calculating the bias. Hence, in this work, we use a fixed observational uncertainty (δ_{obs}) of 5 g m^{-2} while training the emulator. The noise variance was fixed to the ratio $(\delta_{obs}/\sigma_y)^2$, where σ_y is the standard deviation of the training data.

4.1.2 Emulator (b): Time-Averaged Domain-Mean LWP τ Bias

In addition to mean-state cloud amount, realistic simulations must reproduce the temporal evolution and persistence of cloud fields. Cloud lifetime and memory reflect the balance between microphysical processes (e.g., autoconversion and evaporation), turbulent mixing, and mesoscale organization, and therefore provide dynamical information not captured by time-averaged LWP alone. Hence, we further calculated the de-correlation timescales (e-folding time, τ) for the domain-averaged LWP during each phase and for the corresponding observations. De-correlation timescales are instrumental in understanding the evolution and persistence of cloud fields (Gerber et al., 2008; Eastman et al., 2016, 2019, 2021).

We define τ as the e-folding time of the DP-simulated domain-averaged LWP (or observed) time series, derived from the autocorrelation function (ACF):

$$R(\Delta t) = \frac{E[(LWP_t - L\bar{W}P)(LWP_{t+\Delta t} - L\bar{W}P)]}{\sigma^2_{LWP}} \tag{4}$$

where $R(\Delta t)$ is the correlation coefficient at time lag Δt, $E[\cdot]$ denotes the expectation operator over time, $L\bar{W}P$ is the time mean of the domain-averaged LWP, and σ^2_{LWP} is its variance. The timescale τ is identified as the specific lag where $R(\Delta t) = 1/e \approx 0.37$. All calculations are performed at the native 2-minute sampling interval, and the same estimator is applied consistently to simulations and observations.

https://doi.org/10.5194/egusphere-2026-3700
Preprint. Discussion started: 24 July 2026

This metric quantifies the "memory" of the cloud system; a larger τ indicates a more persistent cloud field, while a smaller τ suggests rapid dissipation or high temporal variability. To evaluate the dynamical consistency of the simulations, we define the timescale bias as $\Delta\tau = \tau_{\mathrm{DP}} - \tau_{\mathrm{obs}}$ and train another GPE to predict this bias. This serves as a secondary constraint in our optimization framework to ensure that the selected microphysical parameters produce cloud fields with realistic temporal coherence and to further mitigate parametric equifinality.

Supplement Figure S3 shows the auto-correlation function from the observations and the DP ensemble. It is evident that for the 3 days we simulate, there are multiple timescales in ScP and TrP, possibly due to diurnal cycles and fast turbulence driven processes not simulated by the DP. However, the ScP and TrP phases last only for ~32 and 22 hours; and much longer simulations (and observations) are needed to accurately remove the diurnal cycle. For CuP, the clouds in DP are too persistent and the time scale in the observation is too fast. As a sensitivity test, we repeated the decorrelation-timescale analysis using both a single model grid column and a 15 km × 15 km subdomain centered within the simulation domain. The inferred τ values are sensitive to the spatial averaging scale. Single-column LWP (centre grid box) yields decorrelation timescales of approximately 24 minutes across all three phases with little regime dependence, while the 15 km × 15 km subdomain produces τ values of approximately 38, 40, and 102 minutes for the Sc, Tr, and Cu phases respectively, which is substantially shorter than the full domain-average values of 196, 134, and 164 minutes in the default simulation, but preserving the same qualitative finding of excessive model cloud persistence relative to observations. The shorter single-column timescales likely reflect the passage of individual cloud elements over a fixed location, whereas spatial averaging retains information about cloud-field organization and persistence. Although a single-column metric more closely resembles the instantaneous sampling of the ship, it largely removes the distinction between cloud regimes. In contrast, the spatially averaged metrics preserve the regime-dependent evolution of the simulated cloud field, which is the main quantity of interest in this study. Importantly, the qualitative conclusion that the model exhibits excessive cloud persistence during the cumulus phase remains robust across the different averaging strategies. We also acknowledge that the doubly-periodic setup is neither fully Lagrangian nor Eulerian. Similarly, the direction of the moving ship was such that the air mass sampled by the ship was also different during different hours. The Lagrangian and Eulerian timescales are known to be different (Hanna, 1981; Mauger and Norris, 2010). In spite of several such uncertainties, this metric can introduce a secondary constraint to further address and mitigate parametric uncertainty in simulating the LWP. For example, the temporal autocorrelation for aerosol optical depth have recently been studied by Schutgens et al. (2026), demonstrating the effectiveness of this additional constraint.

τ_{obs} values for Sc, Tr, and Cu phases are 134, 34, and 4 minutes respectively. Unfortunately, all of the τ_{DP} values in the Tr and Cu phases are much larger than the observations, suggesting that microphysics parameters perturbed here cannot explain the model biases during the TrP and CuP. Hence, we decided to train the τ emulator only for the ScP. An initial observational uncertainty of 10 minutes is prescribed during training, after which the GPE adaptively learns the effective uncertainty from the data.

https://doi.org/10.5194/egusphere-2026-3700
Preprint. Discussion started: 24 July 2026

4.2 GPE Training and Analysis

The three primary input parameters (C_{ccn}, C_{auto}, C_{accr}) were logarithmically transformed and standardized prior to training. Once the GPE is trained, we employed a hybrid grid-search and stochastic sampling approach to explore the high-dimensional parameter space of (C_{ccn}, C_{auto}, C_{accr}). For different C_{ccn} values, a log-spaced candidate grid consisting of $N = 100,000$ points in the (C_{auto}, C_{accr}) sub-space was generated using Latin Hypercube sampling. To identify the most robust parameter combinations, we utilized the Expected Absolute Error (EAE) as our objective function. Unlike a simple minimization of the mean bias, the EAE incorporates the emulator's uncertainty, ensuring that selected parameters are both accurate and reliable (See Supplement Text S1 for more details). For each C_{ccn} level (0.5, 0.75, 1, 2, etc) , we retained the subset of $K = 200$ candidates with the lowest EAE. This provides a robust ensemble of low-bias parameter sets for each C_{ccn} value, which were subsequently used for generating relationships among the parameters.

4.3 Extreme Gradient Boosting (XGBoost) and SHapley Additive exPlanations (SHAP) for controlling factors

Extreme Gradient Boosting (XGBoost) is a fast and scalable ML algorithm for supervised learning (Chen and Guestrin, 2016). The XGBoost algorithm (hereafter XGB) can be implemented efficiently in Python, and several studies have used it to study clouds, precipitation, and lightning (Jia et al., 2024; Silva et al., 2022; Andersen et al., 2023; Douglas and L'Ecuyer, 2022; Lin et al., 2024). XGB is particularly effective for structured (tabular) data and supports parallel computation, efficient memory usage, and interpretability. We train a separate XGB for each of the three phases during the SCT.

4.4 XGB Training and Feature Importance Calculation

We use a 'Physics-blocked' cross-validation strategy for XGB training and evaluation. We defined 'extreme physics' as those parameter combinations of (C_{ccn}, C_{accr}, C_{auto}), where at least 2 parameters were either below 15th percentile or above 85th percentile (19 simulations). All the data from the remaining 57 PPE members were used for training and the data from those 19 members were held out for testing. This ensures that the XGB model is evaluated on genuinely unseen regions of parameter space, providing a conservative assessment of out-of-sample skill than the standard k-fold cross-validation. We train an independent XGB model to predict the $\mathrm{LWPB_{DP}}$ for each phase, using domain-averaged DP-simulated physical variables as input. The XGB-predicted $\mathrm{LWPB_{DP}}$ is hereafter referred to simply as LWPB.

To reduce redundancy and mitigate multicollinearity, we first applied a correlation-based filtering step, removing one variable from each highly correlated pair (correlation > 0.7) and retaining the variable with higher mutual information (MI) with the target. The retained variables were then ranked by MI, and the top 10 features were selected. This process was carried out independently for each cloud phase. Table 1 lists all the variables and Supplement Table S1 shows which of them are used in which phase.

Several variables are diagnosed relative to the cloud-top height rather than within the cloud interior. In particular, the inversion strength (`temp_inv`) is defined as the maximum temperature gradient immediately above cloud top, while the cloud-top radiative cooling rate (`rad_cool`) is computed at the cloud top layer. These diagnostics are not subjected to cloud-cover fil-

https://doi.org/10.5194/egusphere-2026-3700
Preprint. Discussion started: 24 July 2026

Table 1. Description of all features used to train the three XGBoost models. All variables are derived from model output between the surface and 3.5 km. Vertical averages are weighted using vertical layer thickness. A cloudy layer is defined as : Liquid Cloud Fraction > 0.1 and Liquid Water Content > 0.01 g kg^{-1}. Not all features are used in each phase (see Supplement Table S1).

Variable	Description
Warm-Rain Microphysics	
`Autoconv`	In-cloud autoconversion rate of cloud water to rain
`Accret`	In-cloud accretion rate of cloud water by rain
`Reff_Liq`	In-cloud effective radius of cloud droplets
`Reff_Rain`	Mean effective radius of rain from cloud top to surface
`nc_incloud`	Cloud droplet number concentration normalized by cloud fraction
`Vap_Liq`	Microphysical vapor–liquid water exchange rate
Cloud-Top Forcing/stability	
`Rad_Cool`	Radiative cooling rate at the cloud top
`Omega`	Pressure vertical velocity at cloud top
`Temp_inv`	Maximum temperature gradient above cloud top (inversion strength)
`Omega_FT`	Pressure vertical velocity at 500 hPa
Surface Coupling & Boundary Layer Dynamics	
`SHF`	Surface sensible heat flux
`LHF`	Surface upward latent heat flux
`Wind_Surf`	Horizontal wind speed at 10 m
`Pblh`	Planetary boundary layer height
`W_Var`	Vertical velocity variance within cloudy grid boxes
Environmental Thermodynamics	
`RH_CT`	Relative humidity sampled above cloud top (10 levels above)
`RH`	In-cloud relative humidity
`Qv`	In-cloud specific humidity
`Qv_2m`	Specific humidity at 2 m altitude

tering, as they represent environmental and cloud-top forcing processes rather than in-cloud properties. Similarly, the planetary boundary layer height (`Pblh`, diagnosed as the height where the bulk Richardson number, computed using virtual potential temperature and wind shear relative to near-surface conditions, first exceeds a critical threshold of 0.3) is used directly as simulated in the DP. Similar variables are important in describing SCTs (Sandu and Stevens, 2011) and some of them have been used in recent studies of LWP evolution during SCTs (Sansom et al., 2026; Erfani et al., 2025) and other ML based studies of cloud properties (Liu et al., 2025).

We calculate feature importance using SHAP (SHapley Additive exPlanations), a cooperative game theory–based framework for explaining machine learning model outputs (Lundberg and Lee, 2017). SHAP assigns each feature an importance value that

https://doi.org/10.5194/egusphere-2026-3700
Preprint. Discussion started: 24 July 2026

reflects its marginal contribution to the prediction, averaged over all possible feature combinations. XGB and SHAP together help us understand the sensitivity of different groups of physical processes (such as microphysics, macrophysics, dynamics, etc.) to the model biases and highlight potential parameterization improvement pathways.

Within each split, we performed 100 bootstrap iterations and calculated SHAP values for each model. Equation 5 expresses the LWPB as the sum of a baseline term and additive feature contributions:

$$\mathrm{LWPB} = \phi_0 + \sum_{i=1}^{N} \phi_i, \tag{5}$$

N is the number of features. where ϕ_0 represents the baseline term, i.e., the expected (mean) LWPB over all training samples, and ϕ_i denotes the contribution of the i^{th} feature. Final feature selection was based on this distribution; specifically, we retained only those features that consistently ranked among the top 6 in terms of SHAP importance (absolute SHAP value) in more than 50% of the bootstrap iterations. We perform a feature importance using the mean and standard deviation of the absolute SHAP values. See Supplement Text S1 for more details.

5 Results

The default DP realistically simulates the SCT event. Supplement Figure S1 shows the evolution of domain averaged relative humidity, liquid water content, temperature, and liquid cloud fraction during the SCT in the default DP simulation.

5.1 Constraining Parameters using the GPEs

Figure 3 shows that the GPE reproduces the LWP bias across the three meteorological regimes with acceptable performance. In the Stratocumulus regime, the emulator achieves exceptional skill with a Leave-One-Out (LOO) cross-validation R^2 of 0.98 and an RMSE of 16.3 g m^{-2}. While the Transition ($R^2 = 0.73$, RMSE = 17.8 g m^{-2}) and Cumulus ($R^2 = 0.83$, RMSE = 7.7 g m^{-2}) phases show moderate GPE performance. Furthermore, the emulator's performance on the secondary constraint, Stratocumulus de-correlation time bias ($\Delta\tau$), yields an R^2 of 0.62 and an RMSE of 16.5 min. Overall, the emulators effectively capture the underlying parametric sensitivity across SCT. Across all panels, the majority of the actual simulation biases fall within the emulator's predictive uncertainty envelope ($\pm 1\sigma$), validating the suitability of the GP for the subsequent analysis.

For each cloud regime, the first two columns of Figure 4 show the contours (response surfaces) of the expected absolute error (EAE) between the emulated and observed LWPB as a function of C_{auto} and C_{accr}, evaluated at fixed $C_{ccn} = 0.5, 1.0$. The EAE metric accounts for both emulator mean bias and predictive uncertainty, providing a probabilistically robust objective surface rather than relying on mean error alone. Regions of low EAE indicate parameter combinations that best minimize the EAE within each cloud regime, i.e. are most plausible. The green dots show the default values of C_{auto} and C_{accr} in the DP.

For the ScP, an additional observational constraint is imposed using an independently trained GP emulator for the ($\Delta\tau$). The dashed contours in panels (a)–(b) denote EAE in $\Delta\tau$, with contour levels at 20, 30, 40, and 50 minutes. The overlap between the regions of lower EAE simultaneously satisfy both LWP and τ constraints. Unlike Schutgens et al. (2026), here the contour

https://doi.org/10.5194/egusphere-2026-3700
Preprint. Discussion started: 24 July 2026

lines of both the constraints are in the same direction, and the overlapping regions are relatively larger. This joint constraint somewhat narrows the viable parameter space, revealing a compensating relationship between C_{auto}, C_{accr}, and C_{ccn}. In the DP-SCREAM simulations, all aerosols available are assumed to activate and form cloud droplets. However, Equation A2 of McGibbon and Bretherton (2017) suggests that only about half of the aerosols are likely to activate during the MAGIC SCT events. The EAE in $\Delta\tau$ is substantially lower for $C_{ccn} = 0.5$ than for $C_{ccn} = 1.0$, with values in the range of 30–40 minutes for $C_{ccn} = 0.5$, increasing to 40–50 minutes for $C_{ccn} = 1.0$. These results indicate that a more consistent and tighter constraint on the parameter space is achieved when using $C_{ccn} = 0.5$, supporting the notion of partial aerosol activation in these conditions. We find a similar region of low LWPB EAE for the TrP, with substantial overlap with the ScP. However, within the explored parameter space, the optimal region for the CuP is very different, favoring much lower autoconversion and accretion rates. This suggests that LWPB in the CuP is more sensitive to other processes like turbulence or boundary layer dynamics, other microphysical parameters or possible structural uncertainties in the DP. Given the proof-of-concept nature of this work, further exploration is left as a part of future work.

The rightmost column quantifies the emergent parameter sensitivity by sampling the top-performing parameter combinations (lowest EAE) and fitting a power-law relationship (linear in log-log space) between C_{auto} and C_{accr} for different C_{ccn} values. Stratocumulus clouds display a tight, nearly linear relationship in log–log space with R^2 scores between 0.9 and 1, indicating a well-defined compensating manifold that shifts systematically with C_{ccn}. This structure weakens in the transition regime and disappears in the cumulus regime, with relatively lower R^2 values. Together, these results demonstrate that optimal microphysical parameters are regime dependent and strongest for stratocumulus clouds, particularly when multiple constraints are applied.

Figure 5 shows the Sobol sensitivity analysis (Sobol, 1993, 2001) quantifying the variance decomposition of the emulator and identifying the relative importance of the parameters. The technique has been described and used in several studies Wong et al. (2025); Sansom et al. (2026); Girard et al. (2016); Marrel et al. (2009). We demonstrate the first-order (S_1) and total-order (S_T) indices. S_1 measures the direct contribution of an individual parameter to the variance of the GPE output, while S_T accounts for both that direct effect and all higher-order interactions with other parameters. In all phases, C_{ccn} is the most dominant source of variance, indicating that the emulator's response is more sensitive to the prescribed droplet number concentrations; this parameter alone explains 50 to 70% of the variability in LWPB in the different phases of the SCT, and almost all of the variability in $\Delta\tau$. The influence of C_{auto} and C_{accr} varies by regime. In the Sc and Cu phases, accretion emerges as the second-most important driver of variance (S_1 about 30%), while autoconversion has the lowest importance. Across the SCT, we find non-negligible non-linear interactions among the microphysical parameters. The total interaction strengths ($\sum(S_T - S_1)$) for all three parameters is about 20% in ScP, 40% in TrP, and 15% in CuP. These interactions are most evident in the emulator's response surfaces (Figure 4), where the distinct curvature and shifting orientation of the bias contours illustrate that the GPE's sensitivity to any single process is fundamentally modulated by the state of the other parameters. Because these sensitivities are interdependent, tuning individual parameters in isolation is insufficient; rather, all three parameters must be optimized simultaneously to improve DP performance.

https://doi.org/10.5194/egusphere-2026-3700
Preprint. Discussion started: 24 July 2026

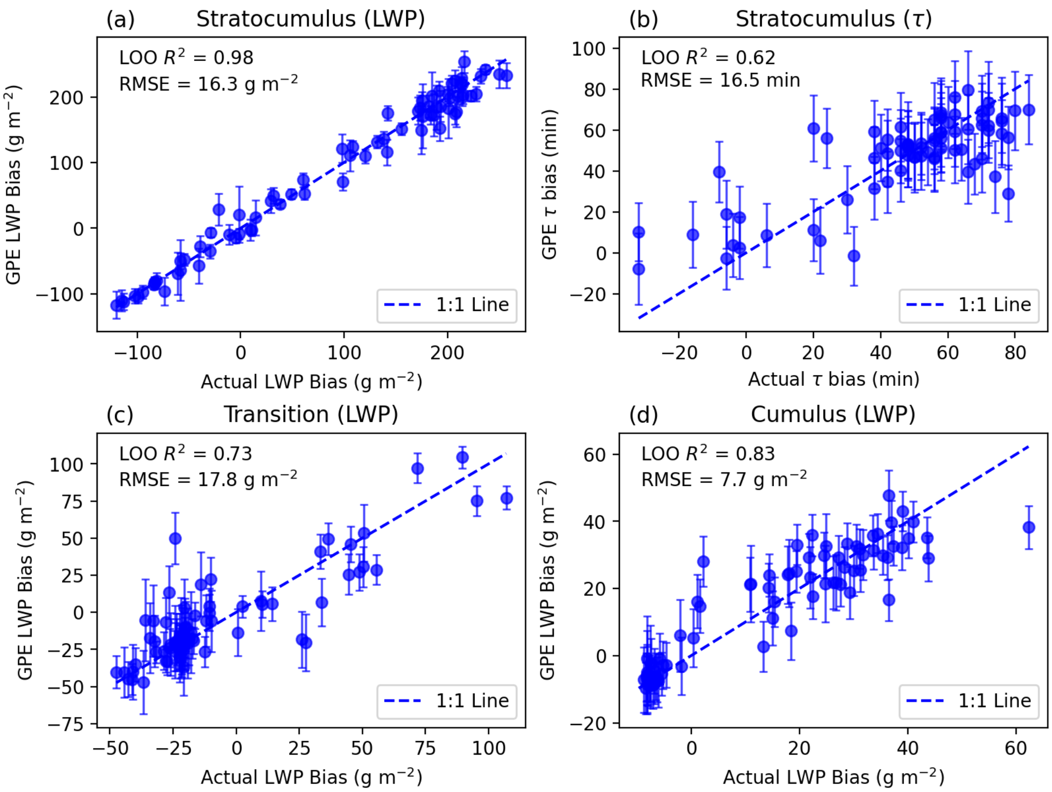

Figure 3. Leave-One-Out (LOO) cross-validation of the Gaussian Process (GP) emulator. The scatter plots compare the actual LWP bias (and the $\Delta\tau$) simulated by DP PPE simulations against the emulator-predicted mean bias (μ) for the (a) Stratocumulus, (b) Transition, and (c) Cumulus regimes. Vertical error bars represent the emulator's predictive uncertainty ($\pm 1\sigma$). The high coefficient of determination (R^2) and alignment of points along the 1:1 dashed line indicate that the emulator accurately captures the parametric sensitivity of the cloud physics across all meteorological phases. For the $\Delta\tau$ emulator only the Stratocumulus phase is shown, as for the other phases, the τ_{obs} was much lower than any of the τ_{DP} from the emulators.

Following this requirement for joint optimization, we investigated whether a shared optimal parameter space exists that satisfies the constraints of multiple regimes. Figure 6 shows cross-regime parametric overlap between ScP and TrP for varying C_{ccn} by simultaneously minimizing the LWPB EAE for both the Stratocumulus and Transition phases. The candidates are also limited to satisfy the physical temporal consistency requirement ($\Delta\tau < 45$ min) within the Stratocumulus regime. A range shift is observed in C_{auto}, which shifts from $1000-2000$ in pristine conditions to > 2500 in polluted environments, while the accretion coefficient C_{accr} varies between 10 and 50.

We conducted a new simulation using the optimal parameters ($C_{ccn} = 0.5$, $C_{auto} = 1410$, and $C_{accr} = 26$; the best candidate in the overlapping region for $C_{ccn} = 0.5$). The DP LWP bias is substantially reduced during the stratocumulus phase (ScP), decreasing from -30.9 g m^{-2} in the default configuration to -0.7 g m^{-2} in the optimized case (Figure 7). A similar

https://doi.org/10.5194/egusphere-2026-3700
Preprint. Discussion started: 24 July 2026

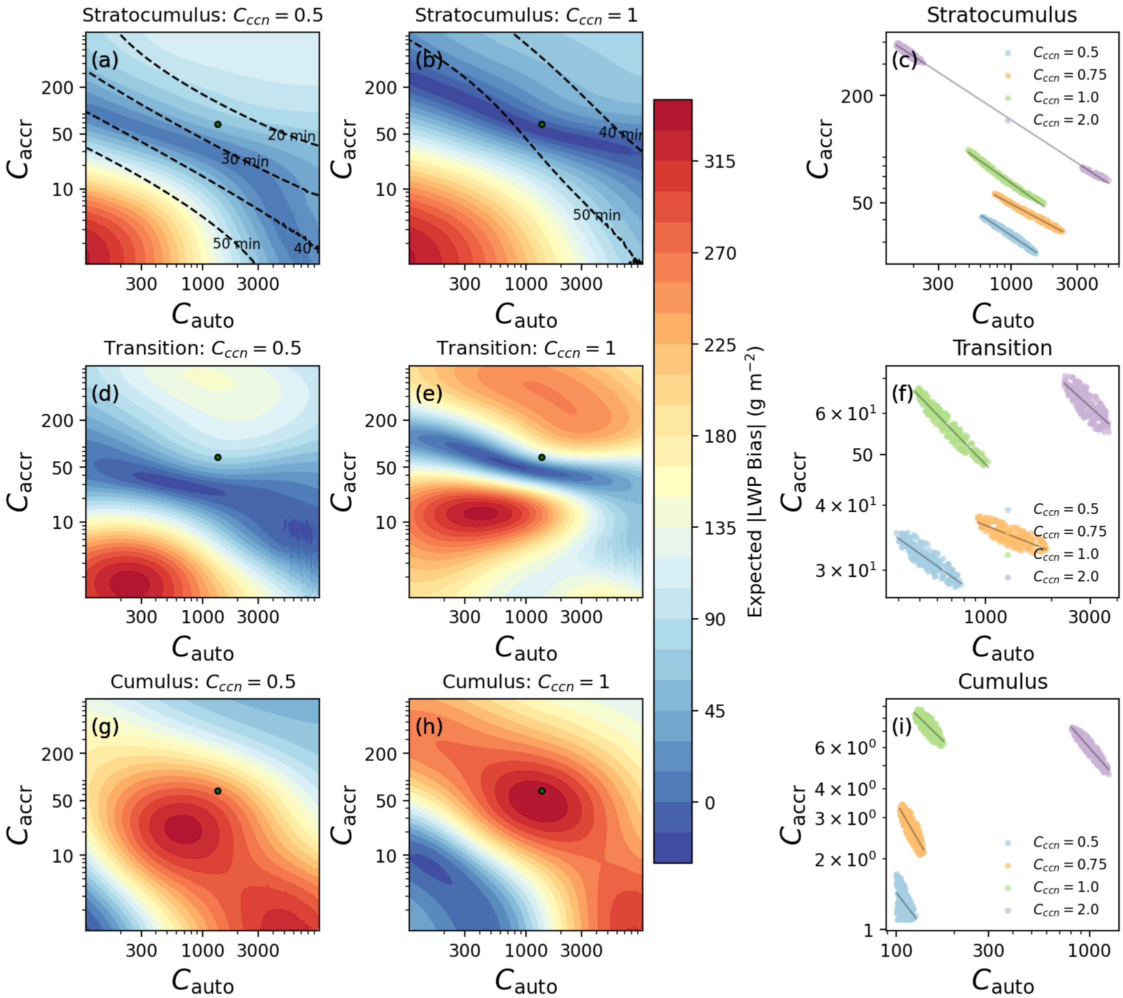

Figure 4. Response surfaces and parametric sensitivity of the Gaussian Process emulators across cloud regimes. Panels (a, b), (d, e), and (g, h) show the acquisition surfaces for the Expected Absolute Error (EAE) of the LWPB as a function of C_{auto} and C_{accr} for $C_{ccn} = 0.5$ and $C_{ccn} = 1.0$ in the Stratocumulus, Transition, and Cumulus regimes, respectively. In panels (a) and (b), the dashed contours denote the Stratocumulus de-correlation timescale difference ($\Delta\tau$) EAE . Panels (c, f, i) display the log-log regression relationships between C_{auto} and C_{accr} for different C_{ccn} groups $(0.5, 0.75, 1.0, 2.0)$. Scatter points represent the top 200 candidate combinations with the lowest EAE for each group, with solid lines indicating the fitted power-law regressions. Green dots show the default value of C_{auto} and C_{accr} in the DP.

improvement is observed during the transition phase (TrP), where the mean bias improves from -22.4 g m^{-2} to 2.8 g m^{-2}. In contrast, the mean LWP bias in the cumulus phase (CuP) does not improve and instead increases from 37.2 g m^{-2} to 46.1 g m^{-2}. The degradation of the Cu phase bias is expected since the overlapped optimal parameters did not include the cumulus phase. As the GPE response surfaces (Figure 4) indicate that the optimal parameter region for the Cu phase differs markedly from that of the Sc and Tr phases, the Cu phase LWP bias is possibly governed by processes beyond warm-rain microphysical

https://doi.org/10.5194/egusphere-2026-3700
Preprint. Discussion started: 24 July 2026

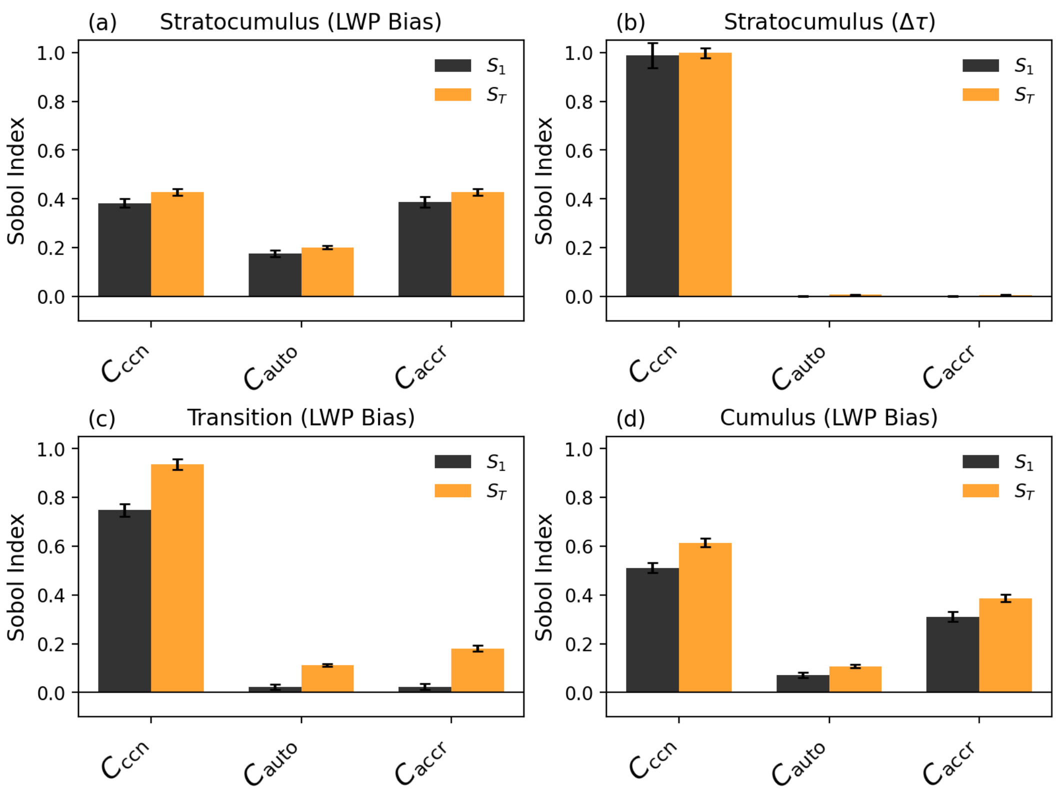

Figure 5. Global sensitivity analysis: Panels show First-order (S_1) and Total-order (S_T) Sobol indices for the Stratocumulus (Both LWPB and $\Delta\tau$), Transition, and Cumulus phases. Error bars denote the 95% confidence intervals estimated via bootstrapping (100 resamples), representing the numerical stability of the variance-based decomposition based on a Saltelli sampling sequence (Saltelli et al., 2010) with a base N=4096 (resulting in N(2k+2)=32768 total evaluations per panel).

parameters alone. The magnitude of the bias is comparable to that reported in previous LES studies of the SCT; for example, McGibbon and Bretherton (2017) reported a mean LWP bias of approximately 4.2 g m^{-2}. As mentioned earlier, we activate 100% of the aerosols. Even when a simplified activation scheme is applied in the DP (or the SCREAM) (Mahfouz et al., 2025, e.g.), the parameter choices of C_{auto} and C_{accr} that are optimal for $C_{ccn} = 1.0$ (Figure 4a) could lead to a large LWPB_{DP} when used with a different value C_{ccn}. To facilitate model portability, Table 2 provides regression-based equations for different C_{ccn}, allowing future users to dynamically adjust microphysical parameters. However, it is important to note that the prescribed CCN itself has uncertainties, since these are climatological mean from 1° global simulations regridded to the DP domain (Donahue et al., 2024). Uncertain prescribed CCNs could lead to compensating biases in other microphysical parameters. Addressing such uncertainties is beyond the scope of this work.

To provide an initial assessment of the transferability of the optimal parameters beyond the MAGIC case, we applied the optimal parameter set ($C_{ccn} = 0.5$, $C_{auto} = 1410$, $C_{accr} = 26$) to an independent DP simulation of a non-precipitating stra-

https://doi.org/10.5194/egusphere-2026-3700
Preprint. Discussion started: 24 July 2026

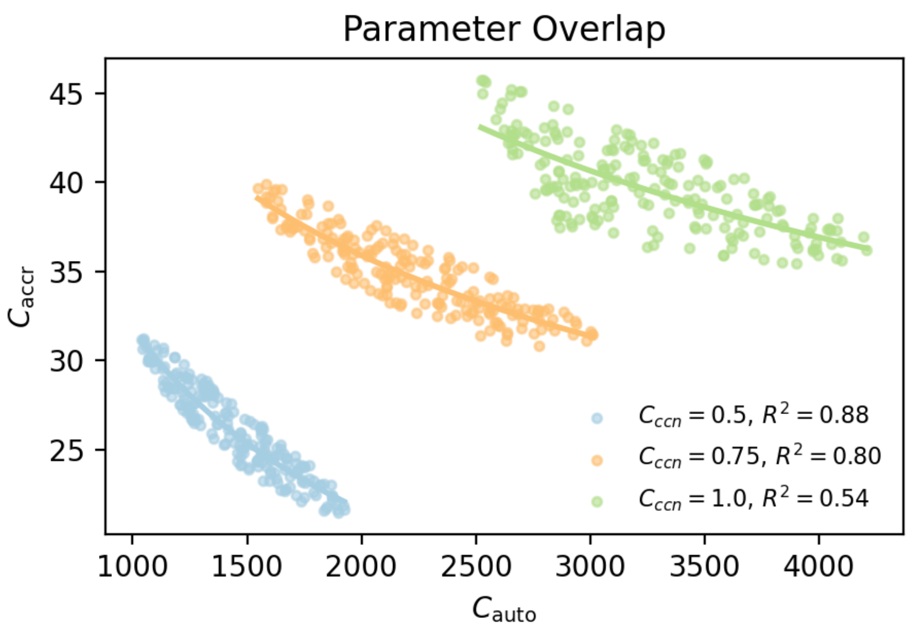

Figure 6. Parameter overlap for Stratocumulus and Transition regimes. Clusters (top 500 cases) indicate parameter sets (C_{auto}, C_{accr}) that minimize LWPB EAE across both phases while satisfying the $\Delta\tau < 40$ min constraint in Sc phase.

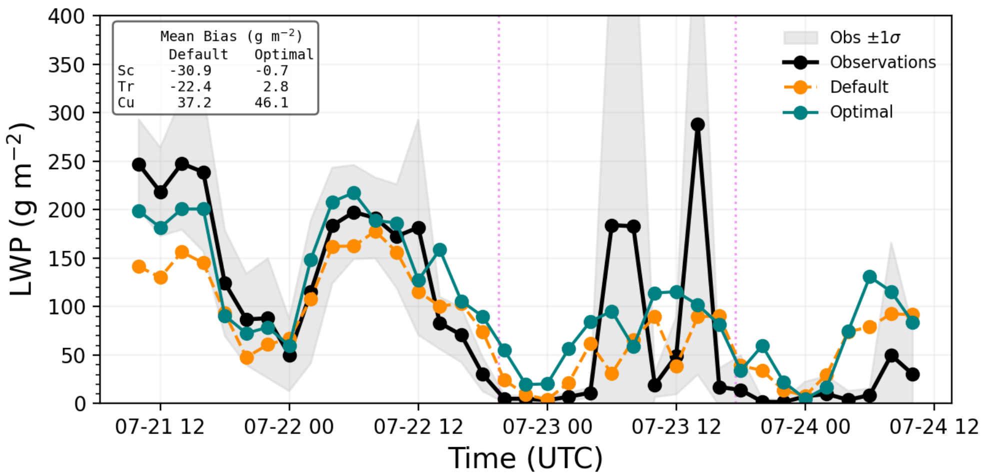

Figure 7. Timeseries of 2-hourly mean LWP from observations, the default simulation and the optimal simulation. The shaded region show 1 standard deviation within that 2-hour period. Vertical purple lines separate stratocumulus, transition, and cumulus phases.

tocumulus case from the Eastern Pacific Cloud Aerosol Precipitation Experiment (EPCAPE), conducted near San Diego, California (Russell et al., 2025, 2021). For our case study (on April 26-28, 2023), in the default configuration, the DP exhibits

https://doi.org/10.5194/egusphere-2026-3700
Preprint. Discussion started: 24 July 2026

Table 2. Power-law regression analysis ($C_{accr} = a \cdot C_{auto}^{b}$) for the identified low-bias parameter overlap between Stratocumulus and Transition phases.

C_{ccn}	Regression Equation	R^2
0.5	$C_{accr} = 1543.973 \cdot C_{auto}^{-0.562}$	0.88
0.75	$C_{accr} = 595.113 \cdot C_{auto}^{-0.369}$	0.80
1.0	$C_{accr} = 733.415 \cdot C_{auto}^{-0.361}$	0.52

a mean LWP bias of -24.0 g m^{-2} during this event (Supplement Figure S5). With the optimal parameters, the mean bias reduces substantially in magnitude to $+16.4$ g m^{-2}, representing a roughly 30% reduction in absolute bias. The sign reversal from negative to slightly positive suggests that while the direction of the bias correction is consistent with the MAGIC-derived optimization, the optimal parameter set retains some case-dependence, which is expected given that the EPCAPE case involves non-precipitating stratocumulus rather than a full SCT event. Nevertheless, the consistent improvement in LWP bias across two independent cases and distinct cloud regimes provides encouraging evidence for the broader applicability of the framework.

Although the GPE allows for a systematic exploration of the parametric sensitivity of the three microphysical parameters, changes in simulated LWP biases cannot be explained solely by the direct impacts of these perturbations on microphysics, because microphysics is rapidly and tightly coupled with precipitation, turbulence, radiation, and the resulting changes in lower-tropospheric conditions. We used the XGB to identify sensitivities of the bias to different microphysical, dynamical, and thermodynamical DP-simulated features to better understand the DP's performance. Comparing these two distinct approaches allows us to confirm whether the diagnostic signatures captured by the XGB align with the underlying parametric sensitivities of the DP's microphysics parameterization.

5.2 Sensitivity of Different Features from XGBoost-SHAP

The scatter plots of XGB predicted versus DP-simulated LWP bias is shown in Figure 8. The XGB models perform well with test-set R^2 of 0.70, 0.53, and 0.74 in ScP, TrP, and CuP, respectively. When normalized by the standard deviation of the DP-simulated LWP bias, the normalized RMSE values are 0.54, 0.58 and 0.51, respectively (higher relative error occurring in the Transition phase, likely due to high LWP peaks of ∼150-250 g m^{-2} on July 23).

Previous studies with XGBoost-SHAP have reported that 40%-70% of the variance can be explained for stratocumulus clouds (Zhang et al., 2024b, 2025), about 55% for Southern Ocean clouds (Fiddes et al., 2024). Gonzalez et al. (2025) has reported an $R^2 > 0.8$ for estimating LWP from satellite observations, with an error of 15%, while Schulte et al. (2024) predicted cloud liquid water content with a correlation co-efficient $R \sim 0.7$. A recent study by Liu et al. (2025) also found $R \sim 0.7$ for ML models used to predict cloud cover. Our results indicate that the feature and LWPB relationship is broadly consistent across extreme and non-extreme physics. Thus, the XGB model is only weakly sensitive to the exact combination of microphysical parameters within the range explored, demonstrating the robustness of the approach.

https://doi.org/10.5194/egusphere-2026-3700
Preprint. Discussion started: 24 July 2026

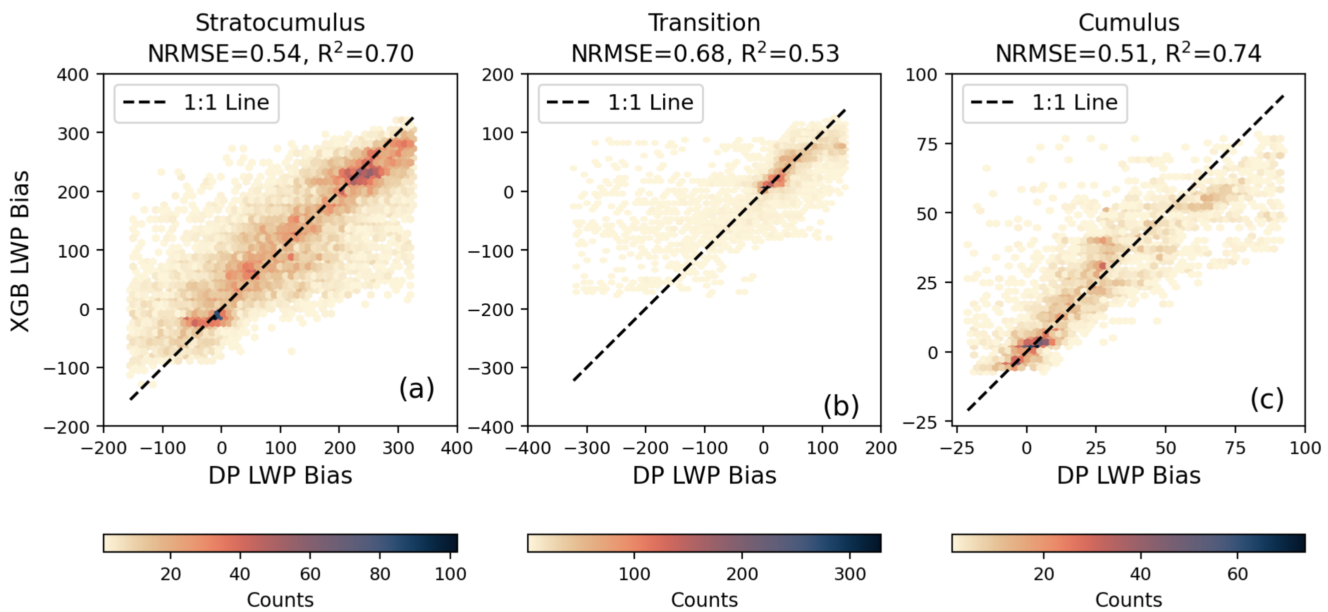

Figure 8. Hexagonal density plots comparing XGB-predicted and DP-simulated liquid water path bias for each phase. Points represent out-of-sample predictions pooled across five physics-blocked shuffle-split cross-validation realizations, with color indicating the number of samples per hexagon. The dashed line denotes the 1:1 relationship.

The perturbed parameters impact the autoconversion and accretion processes as well as droplet number concentrations, directly influencing droplet radius, liquid water path, and precipitation frequency. Variations in cloud liquid water modify cloud-top radiative cooling, which in turn affects cloud-top turbulence and the entrainment of warm, dry air from above the cloud. Changes in entrainment subsequently influence inversion strength and the boundary layer depth.

As cloud properties and boundary-layer structure evolve, surface fluxes are also modified, altering the coupling between the surface and the cloud layer. Through these nonlinear feedbacks, perturbations to a small number of microphysical parameters propagate throughout the coupled cloud–radiation–dynamics system, leading to variability across all predictor variables (Supplement Figure S2) and allowing the ensemble to sample a wide range of dynamically and thermodynamically consistent DP states.

During ScP, the default DP simulation has a LWP mean bias of 30 g m^{-2} for 2-hourly averages (up to 100 g m^{-2} for a particular hour). In the Sc phase, the SHAP analysis indicates that LWP bias is controlled primarily by near-surface moisture availability, with `Qv_2m` emerging as the dominant predictor, followed by in-cloud droplet number `nc_incloud` and accretion rate `Accret`. Contributions from these features range from 20-40 g m^{-2}. This suggests that better representation of the lower boundary-layer moisture supply and its vertical transport into the cloud layer (simulated by SHOC), along with improved representation of microphysical processes governing droplet concentrations and precipitation-related liquid water removal could lead to better simulations of the LWP in the DP.

https://doi.org/10.5194/egusphere-2026-3700
Preprint. Discussion started: 24 July 2026

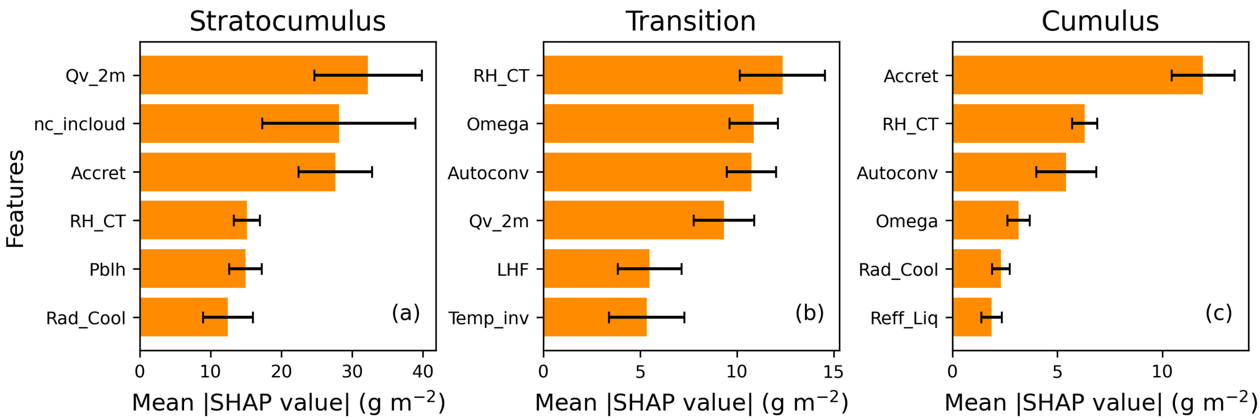

Figure 9. Mean absolute SHAP values (g m^{-2}) for the important predictors of LWPB in the Sc, Tr, and Cu phases. Metrics are aggregated from five physics-blocked cross-validation splits, each containing 100 bootstrap iterations. Features were selected based on a robustness criterion of appearing in the top 6 rankings in $\geq$50% of iterations. Horizontal error bars indicate one standard deviation across all bootstrap members.

Yamaguchi et al. (2017) highlighted that the depletion of aerosols through drizzle scavenging and a faster route to transition, provided that the model accounts for changing droplet number concentrations by collision-coalescence. Van der Dussen et al. (2013) demonstrated a high sensitivity of LWP to differences in the precipitation rate. Stronger precipitating stratocumulus also had reduced warm-air entrainment. Erfani et al. (2022) also showed that the stratocumulus phase is governed by a competition between precipitation efficiency and entrainment drying. Sansom et al. (2026) show the importance of droplet concentrations and autoconversion (their emulator did not have an accretion factor) for SCT. These studies potentially support the importance of droplet concentrations (and other microphysics parameters) in our SHAP rankings during the ScP. Additionally, marine stratocumulus cloud lifecycle are sensitive to cloud-top radiative cooling, driving turbulent mixing and entrainment of free-tropospheric warm air into the boundary layer (Bretherton and Wyant, 1997; Wyant et al., 1997; Bretherton et al., 2004; Wood, 2012), similar to our findings, although with relatively lower sensitivity.

In the TrP, the observations exhibit intermittent periods of high LWP ($>$ 300 g m^{-2}) that are not captured by the model. This discrepancy likely reflects the limitations of the doubly periodic configuration in representing localized, non-repeating cloud structures along the ship track. The SHAP analysis shows that LWP bias is most strongly influenced by `RH_CT` and `Omega`, followed by `Autoconv` and `Qv_2m`. Since `Omega` is calculated specifically at cloud top, its importance indicates that cloud-top dynamical forcing plays a central role in regulating LWP bias during the transition from stratocumulus to more broken cloud fields. Together, the prominence of `RH_CT` and cloud-top `Omega` suggests that the model is especially sensitive to processes near the cloud-top interface, where entrainment, subsidence, and evaporation can strongly modulate cloud thickness and liquid water content. The contribution of `Autoconv` points to the additional influence of microphysical conversion of cloud water to rain, while the continued relevance of `Qv_2m`, `LHF`, and `Temp_inv` indicates that lower-boundary-layer moisture supply and inversion structure still affect the bias, though less strongly than cloud-top thermodynamic and dynamical controls. Overall, the

https://doi.org/10.5194/egusphere-2026-3700
Preprint. Discussion started: 24 July 2026

transition-phase LWP bias appears to be governed mainly by cloud-top humidity and cloud-top vertical motion, with secondary contributions from precipitation formation and sub-cloud moisture conditions.

In the CuP, both observed and simulated mean LWP are substantially lower than ScP; however, the observations exhibit much shorter de-correlation timescales and greater intermittency than the model. LWPB is dominated by `Accret`, with secondary contributions from `RH_CT`, `Autoconv`, and `Omega`. This suggests that, once the cloud field has transitioned to cumulus, the model's LWP bias is governed primarily by microphysical processes that control the growth of precipitation and the removal of cloud liquid water, rather than by lower-boundary-layer moisture supply. The strong importance of `Accret` points to the central role of collision-coalescence and rain growth in regulating how quickly liquid water is depleted from cumulus clouds, while the influence of `Autoconv` further highlights the sensitivity of the bias to parameterized conversion of cloud water into rain. The continued relevance of `RH_CT` and cloud-top `Omega` indicates that thermodynamic and dynamical conditions near cloud top are still important. The smaller but non-negligible contributions from `Rad_Cool` and `Reff_Liq` suggest that radiative effects and droplet size also play supporting roles. Overall, the CuP LWPB appears to reflect a regime in which precipitation-producing microphysics are the dominant control, with cloud-top environment and microphysics providing secondary modulation. This results align well with the GPE, where we found very strong reduction in autoconversion and accretion was needed to reduce the LWP bias.

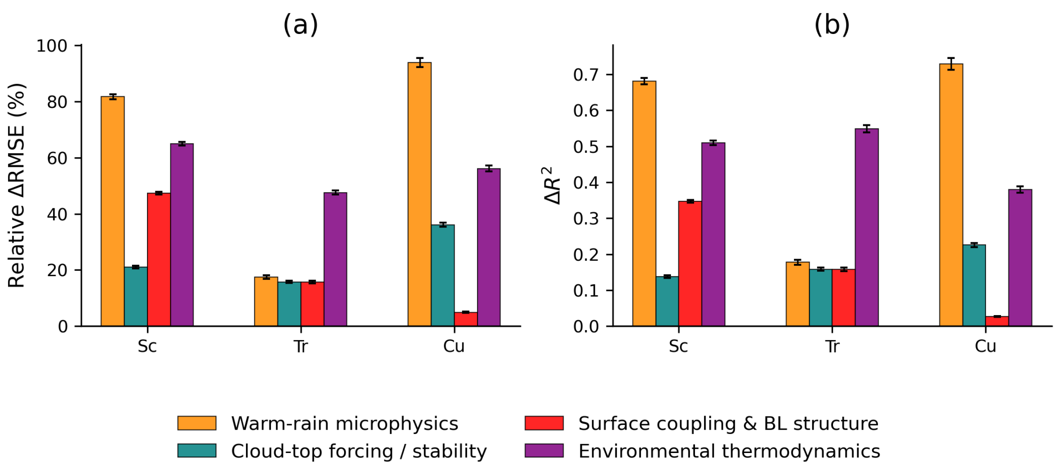

Figure 10. Grouped Permutation Importance for LWP bias across regimes is shown. Panel (a) shows mean increase in Relative RMSE and Panel (b) shows the lowering in R^2 when specific physical process groups are decoupled. $\pm 1\sigma$ over 100 permutations is also shown.

However, all these processes in the DP are coupled together and even if some features do not appear in the top 6, their collective importance could be higher. To further understand the role of different controlling factors, we perform a grouped permutation importance across four groups: Warm-Rain Microphysics, Cloud-Top Forcing/Stability, Environmental Thermodynamics, and Surface Coupling & BL Dynamics (Table 1). This procedure involved randomly shuffling all features within a specific group simultaneously and measuring the resulting degradation in model performance over 100 permutations.

https://doi.org/10.5194/egusphere-2026-3700
Preprint. Discussion started: 24 July 2026

Figure 10 shows that warm-rain microphysics is the dominant predictor in both the stratocumulus ScP and CuP, as expected given the perturbed parameters. In ScP, this category strongly controls model performance, with its perturbation leading to a large degradation in skill ($\Delta R^2 \approx 0.65$) and a $\sim$80% increase in RMSE. Environmental thermodynamics also plays a major secondary role in this phase ($\Delta R^2 \approx 0.5$), followed by surface coupling and boundary-layer (BL) dynamics ($\Delta R^2 \approx 0.3$), highlighting the importance of moisture and surface fluxes in maintaining stratocumulus cloud structure.

As the regime transitions (TrP), the relative importance shifts markedly. Environmental thermodynamics becomes the dominant control ($\Delta R^2 \approx 0.50$), indicating a strong sensitivity to above-cloud humidity and moisture gradients during cloud breakup. In contrast, the contribution of warm-rain microphysics decreases substantially ($\Delta R^2 \approx 0.15$), while surface coupling and BL dynamics ($\Delta R^2 \approx 0.1$) and cloud-top forcing ($\Delta R^2 \approx 0.1$) play comparable but secondary roles. This reflects the increasing influence of large-scale thermodynamic conditions during the stratocumulus-to-cumulus transition.

In the CuP, warm-rain microphysics again emerges as the leading predictor ($\Delta R^2 \approx 0.7$), with environmental thermodynamics as a strong secondary driver ($\Delta R^2 \approx 0.4$). The contributions from cloud-top forcing and surface coupling and BL dynamics are comparatively smaller. This indicates that, while microphysical processes dominate variability in the cumulus regime, moisture and thermodynamic controls remain important, whereas dynamical and cloud-top processes play a reduced role.

Overall, this grouped analysis highlights a clear regime-dependent shift in controlling processes: from microphysics-dominated behavior in the stratocumulus phase, to thermodynamically controlled variability in the transition phase, and back to a combination of microphysical and thermodynamic controls in the cumulus regime. By accounting for inter-variable correlations within each physical group, this approach demonstrates that, beyond microphysics, environmental thermodynamics consistently exerts a strong influence, particularly as the boundary layer deepens and decouples.

5.3 Cloud Radiative Effects

In the default DP configuration, the shortwave cloud radiative effect (CRE) is –112.9, –38.2, and –37.5 W m^{-2} for the stratocumulus, transition, and cumulus phases, respectively. In the optimal configuration, these values strengthen to –122.1, –43.0, and –45.2 W m^{-2}. In contrast, the longwave component exhibits only minor changes across all phases (within $\sim$1 W m^{-2}). Consequently, the domain-mean net CRE increases in magnitude from –61.4 W m^{-2} in the default simulation to –68.5 W m^{-2} in the optimal configuration, corresponding to an enhancement of approximately 12%, driven primarily by stronger shortwave cloud cooling. Because the prescribed droplet number concentrations are different between simulations, these changes could be due to a combination of the Twomey effect and the cloud lifetime effect.

Supplement Figure S6 shows the SW, LW and net CRE from the CERES-EBAF 4.2 satellite product (Loeb et al., 2018) for July 2013. During that time, the average SW, LW and net CRE is estimated to be -73, 14, and -59 Wm^{-2} respectively, calculated using the band from the start location of the simulation to the end location of the simulation following the ship track as shown in Zheng et al. (2020). Although an exact comparison of the 3 km spacing DP simulations with the 1°CERES observations is uncertain, Terai et al. (2025) showed that the SCREAM model exhibits a regional underestimation of shortwave CRE in the eastern Pacific stratocumulus deck, consistent with weaker cloud albedo in this region. Similarly, Nowak et al. (2025)

https://doi.org/10.5194/egusphere-2026-3700
Preprint. Discussion started: 24 July 2026

found that simplified parameterizations underestimate albedo in the SCT region near the California coast. Since our optimal simulation strengthens the SW CRE, it could possibly lead to model improvements. However, long term multi-year global simulations are needed for an accurate comparison, which is left as a part of future work.

6 Discussion and Conclusions

We integrate ARM observations into two independent ML frameworks to understand the sensitivities of the DP-EAMxx model during different phases of an SCT event. We use separate GPEs for LWP bias and LWP decorrelation timescale bias to explore the parametric sensitivity of the warm-rain microphysics. The GPEs identify a narrow, physically interpretable manifold of parameter combinations that minimize the expected absolute error in the ScP and TrP. These results suggest that reducing either autoconversion or accretion, for a fixed droplet concentration, can improve model performance in these regimes. In contrast, the CuP requires a substantially larger reduction in both autoconversion and accretion, and the region of minimal absolute bias differs markedly from that of the ScP and TrP, indicating that the low-bias microphysical parameter space is regime dependent.

The persistence of the clouds is much higher in the DP during TrP and CuP than in the observations. Sobol analysis further demonstrates the importance of droplet number concentration in all phases, along with substantial parameter interaction effects, also reflected in the nonlinear acquisition surfaces of the GPE. Using the overlapping optimal parameter set from the Sc and Tr phases, the mean LWP bias improves from -31 and -22 g m^{-2} to -1 and 3 g m^{-2} in the Sc and Tr phases, respectively, but degrades in the Cu phase. This highlights the difficulty of simultaneously representing all three regimes using the explored parameter combinations.

Based on these findings, we next examine sensitivities using XGBoost-SHAP analysis. Consistent with the GPE results, we find high sensitivity of LWP bias to droplet number concentration in the ScP. However, along with microphysics, several dynamical, cloud-top forcing, and thermodynamical features are also important in the other phases.

Although the GPE-Sobol and XGB-SHAP analyses together identify important sensitivities of LWPB, improving DP parameterizations remains a longer-term effort beyond the scope of the present study. In spite of several uncertainties, our analysis is robust to choices of kernel, subsampling, and domain size (Supplement Text S2). Our results suggest that reducing LWP bias in a storm-resolving model will likely require developments beyond tuning of the explored warm-rain microphysical parameters, as evidenced by the inability of the optimal parameter combinations to simultaneously improve all three SCT phases, itself a key diagnostic finding of this study, in line with Chun et al. (2025); Stevens and Feingold (2009). The Cu phase degradation is not simply a failure of the optimization framework, but rather a diagnostic signal: the regime-dependent shift in controlling processes identified by both the GPE-Sobol and XGBoost-SHAP analyses suggests that Cu phase biases are influenced by factors beyond the explored warm-rain parameter subset and may also reflect broader limitations in the current model formulation. This is the type of distinction the framework is intended to help diagnose, and we suggest that addressing Cu phase biases may require further tuning and future developments in turbulence and boundary layer parameterizations following Zhang et al. (2026).

https://doi.org/10.5194/egusphere-2026-3700
Preprint. Discussion started: 24 July 2026

The novelty of this study lies in the integration of XGBoost-SHAP and Gaussian process emulators within a physics-blocked PPE framework to diagnose model sensitivities in a physically interpretable way. Feature selection based on correlation and mutual information reduces redundancy while retaining relevant predictors, and the use of separate models for each cloud phase allows regime-dependent sensitivities to be isolated clearly. In addition, developing distinct GPEs for LWP bias and LWP decorrelation timescale bias enables us to assess both mean-state and persistence-related model errors. Together, these elements provide a flexible and computationally efficient framework for observation-constrained diagnosis of cloud-regime-specific model deficiencies.

A key question for any single-case modeling study is the extent to which the findings generalize beyond the specific event analyzed. The MAGIC leg 15A case was selected because it is one of the best-observed SCT events available, making it well suited for a proof-of-concept study. However, SCT events can differ substantially in aerosol loading, inversion strength, and large-scale subsidence, all of which could modulate the regime-dependent parameter sensitivities identified here. The EPCAPE result discussed in Section 5.1 provides an initial indication that the bias reduction achieved through the optimization of microphysical parameters is not entirely specific to the MAGIC case. We emphasize that the primary contribution of this work is not the identification of a universally optimal parameter set, but rather the demonstration of a scalable, physically interpretable framework for diagnosing whether model biases are primarily parametric or reflect broader model limitations. Future work applying this framework to additional cases, cloud regimes, and parameter subsets will be needed to better characterize its generalization.

Code and data availability. EAMxx is open-source and the latest code is available at: https://github.com/E3SM-Project/E3SM (Last Access: Jun 23, 2026). Model data, observations, and code used in this study can be found at: https://doi.org/10.5281/zenodo.20804376 (Ghosh and Zheng, 2026).

Author contributions. PG and XZ developed the idea of the manuscript. PG ran all simulations. PG wrote this paper with comments and suggestions from all co-authors.

Competing interests. The authors declare no competing interest.

Acknowledgements. This work is supported by the DOE Office of Science Early Career Research Program. This work was performed under the auspices of the U.S. Department of Energy by Lawrence Livermore National Laboratory under Contract DE-AC52-07NA27344 (IM: LLNL-JRNL-2016442). All simulations were performed on a high-performance computing cluster provided by the National Energy Research Scientific Computing Center (NERSC), a DOE Office of Science User Facility supported by the Office of Science of the US Department of Energy under contract no. DE-AC02-05CH11231. We thank the scientists responsible for the MAGIC field campaign for producing high-

https://doi.org/10.5194/egusphere-2026-3700
Preprint. Discussion started: 24 July 2026

quality observational data. We acknowledge the use of imagery from the NASA Worldview application (https://worldview.earthdata.nasa.gov), part of the NASA Earth Science Data and Information System (ESDIS). H. Beydoun, P. Bogenschutz and Y. Zhang acknowledge support from DOE Atmospheric System Research Tying in High Resolution E3SM with ARM Data (THREAD) project.

https://doi.org/10.5194/egusphere-2026-3700
Preprint. Discussion started: 24 July 2026

References

Andersen, H., Cermak, J., Douglas, A., Myers, T. A., Nowack, P., Stier, P., Wall, C. J., and Wilson Kemsley, S.: Sensitivities of cloud radiative effects to large-scale meteorology and aerosols from global observations, Atmospheric Chemistry and Physics, 23, 10 775–10 794, https://doi.org/10.5194/acp-23-10775-2023, 2023.

Bertagna, L., Guba, O., Taylor, M. A., Foucar, J. G., Larkin, J., Bradley, A. M., et al.: A performance-portable nonhydrostatic atmospheric dycore for the energy exascale earth system model running at cloud-resolving resolutions, in: SC20: International Conference for High Performance Computing, Networking, Storage and Analysis, pp. 1–14, https://doi.org/10.1109/SC41405.2020.00096, 2020.

Bogenschutz, P. A. and Krueger, S. K.: A simplified PDF parameterization of subgrid-scale clouds and turbulence for cloud-resolving models, Journal of Advances in Modeling Earth Systems, 5, 195–211, 2013.

Bogenschutz, P. A., Gettelman, A., Morrison, H., Larson, V. E., Craig, C., and Schanen, D. P.: Higher-order turbulence closure and its impact on climate simulations in the Community Atmosphere Model, Journal of Climate, 26, 9655–9676, 2013.

Bogenschutz, P. A., Eldred, C., and Caldwell, P. M.: Horizontal Resolution Sensitivity of the Simple Convection-Permitting E3SM Atmosphere Model in a Doubly-Periodic Configuration, Journal of Advances in Modeling Earth Systems, 15, e2022MS003 466, https://doi.org/https://doi.org/10.1029/2022MS003466, e2022MS003466 2022MS003466, 2023.

Bogenschutz, P. A., Zhang, Y., Zheng, X., Tian, Y., Zhang, M., Lin, L., Wu, P., Xie, S., and Tao, C.: Exposing Process-Level Biases in a Global Cloud Permitting Model With ARM Observations, Journal of Geophysical Research: Atmospheres, 130, e2024JD043 059, https://doi.org/https://doi.org/10.1029/2024JD043059, e2024JD043059 2024JD043059, 2025.

Bretherton, C.: A conceptual model of the stratocumulus-trade-cumulus transition in the subtropical oceans, in: Proc. 11th Int. Conf. on Clouds and Precipitation, vol. 1, pp. 374–377, 1992.

Bretherton, C. S.: Insights into low-latitude cloud feedbacks from high-resolution models, Philosophical Transactions of the Royal Society A: Mathematical, Physical and Engineering Sciences, 373, 20140 415, 2015.

Bretherton, C. S. and Wyant, M. C.: Moisture Transport, Lower-Tropospheric Stability, and Decoupling of Cloud-Topped Boundary Layers, Journal of the Atmospheric Sciences, 54, 148 – 167, https://doi.org/10.1175/1520-0469(1997)054<0148:MTLTSA>2.0.CO;2, 1997.

Bretherton, C. S., Uttal, T., Fairall, C. W., Yuter, S. E., Weller, R. A., Baumgardner, D., Comstock, K., Wood, R., and Raga, G. B.: The Epic 2001 Stratocumulus Study, Bulletin of the American Meteorological Society, 85, 967 – 978, https://doi.org/10.1175/BAMS-85-7-967, 2004.

Cadeddu, M., Liljegren, J., and Turner, D.: The Atmospheric Radiation Measurement (ARM) program network of microwave radiometers: Instrumentation, data, and retrievals, Atmospheric Measurement Techniques Discussions, 6, 3723–3763, 2013.

Caldwell, P. M., Terai, C. R., Hillman, B., Keen, N. D., Bogenschutz, P., Lin, W., et al.: Convection-permitting simulations with the E3SM global atmosphere model, Journal of Advances in Modeling Earth Systems, 13, e2021MS002 544, https://doi.org/10.1029/2021MS002544, 2021.

Carslaw, K. S., Regayre, L. A., Proske, U., Gettelman, A., Sexton, D. M. H., Qian, Y., Marshall, L. R., Wild, O., van Lier-Walqui, M., Oertel, A., Peatier, S., Yang, B., Johnson, J. S., Li, S., McCoy, D. T., Sanderson, B. M., Williamson, C. J., Elsaesser, G. S., Yamazaki, K., and Booth, B. B. B.: Opinion: The importance and future development of perturbed parameter ensembles in climate and atmospheric science, Atmospheric Chemistry and Physics, 26, 4651–4667, https://doi.org/10.5194/acp-26-4651-2026, 2026.

https://doi.org/10.5194/egusphere-2026-3700
Preprint. Discussion started: 24 July 2026

Chen, T. and Guestrin, C.: XGBoost: A Scalable Tree Boosting System, in: Proceedings of the 22nd ACM SIGKDD International Conference on Knowledge Discovery and Data Mining, KDD '16, p. 785–794, Association for Computing Machinery, New York, NY, USA, ISBN 9781450342322, https://doi.org/10.1145/2939672.2939785, 2016.

Chen, T., Rossow, W. B., and Zhang, Y.: Radiative Effects of Cloud-Type Variations, Journal of Climate, 13, 264 – 286, https://doi.org/10.1175/1520-0442(2000)013<0264:REOCTV>2.0.CO;2, 2000.

Chun, J.-Y., Wood, R., Blossey, P. N., and Doherty, S. J.: Impact on the Stratocumulus-to-Cumulus Transition of the Interaction of Cloud Microphysics and Macrophysics with Large-Scale Circulation, Atmospheric Chemistry and Physics, 25, 5251–5271, https://doi.org/10.5194/acp-25-5251-2025, 2025.

Dennis, J., Fournier, A., Spotz, W. F., St-Cyr, A., Taylor, M. A., Thomas, S. J., and Tufo, H.: High-resolution mesh convergence properties and parallel efficiency of a spectral element atmospheric dynamical core, International Journal of High Performance Computing Applications, 19, 225–235, https://doi.org/10.1177/1094342005056108, 2005.

Dennis, J., Edwards, J., Evans, K. J., Guba, O., Lauritzen, P., Mirin, A. A., et al.: CAM-SE: A scalable spectral element dynamical core for the Community Atmosphere Model, International Journal of High Performance Computing Applications, 26, 74–89, https://doi.org/10.1177/1094342011428142, 2012.

Diamond, M. S., Saide, P. E., Zuidema, P., Ackerman, A. S., Doherty, S. J., Fridlind, A. M., Gordon, H., Howes, C., Kazil, J., Yamaguchi, T., Zhang, J., Feingold, G., and Wood, R.: Cloud adjustments from large-scale smoke–circulation interactions strongly modulate the southeastern Atlantic stratocumulus-to-cumulus transition, Atmospheric Chemistry and Physics, 22, 12 113–12 151, https://doi.org/10.5194/acp-22-12113-2022, 2022.

Donahue, A. S., Caldwell, P. M., Bertagna, L., Beydoun, H., Bogenschutz, P. A., Bradley, A. M., Clevenger, T. C., Foucar, J., Golaz, C., Guba, O., Hannah, W., Hillman, B. R., Johnson, J. N., Keen, N., Lin, W., Singh, B., Sreepathi, S., Taylor, M. A., Tian, J., Terai, C. R., Ullrich, P. A., Yuan, X., and Zhang, Y.: To Exascale and Beyond—The Simple Cloud-Resolving E3SM Atmosphere Model (SCREAM), a Performance Portable Global Atmosphere Model for Cloud-Resolving Scales, Journal of Advances in Modeling Earth Systems, 16, e2024MS004 314, https://doi.org/https://doi.org/10.1029/2024MS004314, e2024MS004314 2024MS004314, 2024.

Douglas, A. R. and L'Ecuyer, T.: Possible evidence of increased global cloudiness due to aerosol-cloud interactions, Atmospheric Chemistry and Physics Discussions, https://doi.org/10.5194/acp-2022-688, [preprint], 2022.

Eastman, R., Wood, R., and Bretherton, C. S.: Time Scales of Clouds and Cloud-Controlling Variables in Subtropical Stratocumulus from a Lagrangian Perspective, Journal of the Atmospheric Sciences, 73, 3079 – 3091, https://doi.org/10.1175/JAS-D-16-0050.1, 2016.

Eastman, R., Lebsock, M., and Wood, R.: Warm rain rates from AMSR-E 89-GHz brightness temperatures trained using CloudSat rain-rate observations, Journal of Atmospheric and Oceanic Technology, 36, 1033–1051, 2019.

Eastman, R., Terai, C. R., Grosvenor, D. P., and Wood, R.: Evaluating the Lagrangian Evolution of Subtropical Low Clouds in GCMs Using Observations: Mean Evolution, Time Scales, and Responses to Predictors, Journal of the Atmospheric Sciences, 78, 353 – 372, https://doi.org/10.1175/JAS-D-20-0178.1, 2021.

Erfani, E., Blossey, P., Wood, R., Mohrmann, J., Doherty, S. J., Wyant, M., and O, K.-T.: Simulating Aerosol Lifecycle Impacts on the Subtropical Stratocumulus-to-Cumulus Transition Using Large-Eddy Simulations, Journal of Geophysical Research: Atmospheres, 127, e2022JD037 258, https://doi.org/https://doi.org/10.1029/2022JD037258, e2022JD037258 2022JD037258, 2022.

Erfani, E., Wood, R., Blossey, P., Doherty, S. J., and Eastman, R.: Building a comprehensive library of observed Lagrangian trajectories for testing modeled cloud evolution, aerosol–cloud interactions, and marine cloud brightening, Atmospheric Chemistry and Physics, 25, 8743–8768, https://doi.org/10.5194/acp-25-8743-2025, 2025.

https://doi.org/10.5194/egusphere-2026-3700
Preprint. Discussion started: 24 July 2026

Fiddes, S. L., Mallet, M. D., Protat, A., Woodhouse, M. T., Alexander, S. P., and Furtado, K.: A machine learning approach for evaluating Southern Ocean cloud radiative biases in a global atmosphere model, Geoscientific Model Development, 17, 2641–2662, https://doi.org/10.5194/gmd-17-2641-2024, 2024.

Fuchs, D., Sherwood, S. C., Prasad, A., Trapeznikov, K., and Gimlett, J.: TorchClim v1.0: a deep-learning plugin for climate model physics, Geoscientific Model Development, 17, 5459–5475, https://doi.org/10.5194/gmd-17-5459-2024, 2024.

Gerber, E. P., Voronin, S., and Polvani, L. M.: Testing the Annular Mode Autocorrelation Time Scale in Simple Atmospheric General Circulation Models, Monthly Weather Review, 136, 1523 – 1536, https://doi.org/10.1175/2007MWR2211.1, 2008.

Gettelman, A., Gagne, D. J., Chen, C.-C., Christensen, M. W., Lebo, Z. J., Morrison, H., and Gantos, G.: Machine Learning the Warm Rain Process, Journal of Advances in Modeling Earth Systems, 13, e2020MS002 268, https://doi.org/https://doi.org/10.1029/2020MS002268, e2020MS002268 2020MS002268, 2021.

Ghate, V. P. and Cadeddu, M. P.: Drizzle and turbulence below closed cellular marine stratocumulus clouds, Journal of Geophysical Research: Atmospheres, 124, 5724–5737, 2019.

Ghate, V. P., Mechem, D. B., Cadeddu, M. P., Eloranta, E. W., Jensen, M. P., Nordeen, M. L., and Smith Jr, W. L.: Estimates of entrainment in closed cellular marine stratocumulus clouds from the MAGIC field campaign, Quarterly Journal of the Royal Meteorological Society, 145, 1589–1602, https://doi.org/https://doi.org/10.1002/qj.3514, 2019.

Ghosh, P. and Zheng, X.: Dataset and Code for "Towards Better Simulations of Liquid Water Path during Stratocumulus-to- Cumulus Transition: Insights from Gaussian Process Emulator, XGBoost and MAGIC Observations", https://doi.org/10.5281/zenodo.20804376, 2026.

Ghosh, P., Boutle, I., Field, P., Hill, A., Mazoyer, M., Evans, K. J., Mahajan, S., Kang, H.-G., Xu, M., Zhang, W., and Gordon, H.: Adiabatic and radiative cooling are both important causes of aerosol activation in simulated fog events in Europe, Atmospheric Chemistry and Physics, 25, 11 157–11 182, https://doi.org/10.5194/acp-25-11157-2025, 2025.

Girard, S., Mallet, V., Korsakissok, I., and Mathieu, A.: Emulation and Sobol'sensitivity analysis of an atmospheric dispersion model applied to the Fukushima nuclear accident, Journal of Geophysical Research: Atmospheres, 121, 3484–3496, 2016.

Gonzalez, J., Dipu, S., Jimenez, G., Camps-Valls, G., and Quaas, J.: Machine Learning-Based Retrieval of Cloud Droplet Number Concentration and Liquid Water Path From Satellite Spectral Data, IEEE Journal of Selected Topics in Applied Earth Observations and Remote Sensing, 2025.

Gordon, H., Field, P. R., Abel, S. J., Barrett, P., Bower, K., Crawford, I., Cui, Z., Grosvenor, D. P., Hill, A. A., Taylor, J., Wilkinson, J., Wu, H., and Carslaw, K. S.: Development of aerosol activation in the double-moment Unified Model and evaluation with CLARIFY measurements, Atmospheric Chemistry and Physics, 20, 10 997–11 024, https://doi.org/10.5194/acp-20-10997-2020, 2020.

Grosvenor, D. P. and Carslaw, K. S.: The decomposition of cloud–aerosol forcing in the UK Earth System Model (UKESM1), Atmospheric Chemistry and Physics, 20, 15 681–15 724, https://doi.org/10.5194/acp-20-15681-2020, 2020.

Hanna, S. R.: Lagrangian and Eulerian time-scale relations in the daytime boundary layer, Journal of Applied Meteorology, 20, 242–249, https://doi.org/10.1175/1520-0450(1981)020<0242:LAETSR>2.0.CO;2, 1981.

Hartmann, D. L. and Short, D. A.: On the Use of Earth Radiation Budget Statistics for Studies of Clouds and Climate, Journal of Atmospheric Sciences, 37, 1233 – 1250, https://doi.org/10.1175/1520-0469(1980)037<1233:OTUOER>2.0.CO;2, 1980.

Helton, J. and Davis, F.: Latin hypercube sampling and the propagation of uncertainty in analyses of complex systems, Reliability Engineering & System Safety, 81, 23–69, https://doi.org/https://doi.org/10.1016/S0951-8320(03)00058-9, 2003.

https://doi.org/10.5194/egusphere-2026-3700
Preprint. Discussion started: 24 July 2026

Jia, Y., Andersen, H., and Cermak, J.: Analysis of the cloud fraction adjustment to aerosols and its dependence on meteorological controls using explainable machine learning, Atmospheric Chemistry and Physics, 24, 13 025–13 045, https://doi.org/10.5194/acp-24-13025-2024, 2024.

Jian, B., Li, J., Wang, G., Zhao, Y., Li, Y., Wang, J., Zhang, M., and Huang, J.: Evaluation of the CMIP6 marine subtropical stratocumulus cloud albedo and its controlling factors, Atmospheric Chemistry and Physics Discussions, 2021, 1–29, 2021.

Khairoutdinov, M. and Kogan, Y.: A New Cloud Physics Parameterization in a Large-Eddy Simulation Model of Marine Stratocumulus, Monthly Weather Review, 128, 229 – 243, https://doi.org/10.1175/1520-0493(2000)128<0229:ANCPPI>2.0.CO;2, 2000.

Li, S., Rupp, D. E., Hawkins, L., Mote, P. W., McNeall, D., Sparrow, S. N., Wallom, D. C. H., Betts, R. A., and Wettstein, J. J.: Reducing climate model biases by exploring parameter space with large ensembles of climate model simulations and statistical emulation, Geoscientific Model Development, 12, 3017–3043, https://doi.org/10.5194/gmd-12-3017-2019, 2019.

Lin, J.-L., Qian, T., and Shinoda, T.: Stratocumulus clouds in Southeastern Pacific simulated by eight CMIP5–CFMIP global climate models, Journal of Climate, 27, 3000–3022, 2014.

Lin, X., Fan, J., Zhang, Y., and Hou, Z.: Machine Learning Analysis of Impact of Western US Fires on Central US Hailstorms, Advances in Atmospheric Sciences, 41, 1–13, https://doi.org/10.1007/s00376-024-3198-7, 2024.

Liu, Z., Eastman, R., and Wood, R.: A Machine Learning Approach to Cloud Cover Forecasting Using Lagrangian Air Mass History, Authorea Preprints, 2025.

Loeb, N. G., Doelling, D. R., Wang, H., Su, W., Nguyen, C., Corbett, J. G., Liang, L., Mitrescu, C., Rose, F. G., and Kato, S.: Clouds and the Earth's Radiant Energy System (CERES) Energy Balanced and Filled (EBAF) Top-of-Atmosphere (TOA) Edition-4.0 Data Product, Journal of Climate, 31, 895–918, https://doi.org/10.1175/JCLI-D-17-0208.1, 2018.

Lohmann, U.: Possible Aerosol Effects on Ice Clouds via Contact Nucleation, Journal of the Atmospheric Sciences, 59, 647 – 656, https://doi.org/10.1175/1520-0469(2001)059<0647:PAEOIC>2.0.CO;2, 2002.

Lundberg, S. M. and Lee, S.-I.: A Unified Approach to Interpreting Model Predictions, in: Advances in Neural Information Processing Systems, edited by Guyon, I., Luxburg, U. V., Bengio, S., Wallach, H., Fergus, R., Vishwanathan, S., and Garnett, R., vol. 30, Curran Associates, Inc., https://proceedings.neurips.cc/paper_files/paper/2017/file/8a20a8621978632d76c43dfd28b67767-Paper.pdf, 2017.

M. D. Mckay, R. J. B. and Conover, W. J.: A Comparison of Three Methods for Selecting Values of Input Variables in the Analysis of Output From a Computer Code, Technometrics, 42, 55–61, https://doi.org/10.1080/00401706.2000.10485979, 2000.

Mahfouz, N., Beydoun, H., Mülmenstädt, J., Keen, N., Varble, A. C., Bertagna, L., Bogenschutz, P., Bradley, A., Christensen, M. W., Clevenger, T. C., Donahue, A., Fast, J., Foucar, J., Golaz, J.-C., Guba, O., Hannah, W., Hillman, B., Jacob, R., Lin, W., Ma, P.-L., Qian, Y., Singh, B., Terai, C., Wang, H., Wu, M., Zhang, K., Gettelman, A., Taylor, M., Leung, L. R., Caldwell, P., and Burrows, S.: Prescribing the aerosol effective radiative forcing in the Simple Cloud-Resolving E3SM Atmosphere Model v1, EGUsphere, https://doi.org/10.5194/egusphere-2025-1868, preprint, 2025.

Makgoale, T. E. and Sullivan, S. C.: Characterization and comparison of simulated precipitation efficiency from global storm-resolving models over the Asian monsoon region, Journal of Geophysical Research: Atmospheres, 130, e2025JD044 228, https://doi.org/10.1029/2025JD044228, 2025.

Marrel, A., Iooss, B., Laurent, B., and Roustant, O.: Calculations of Sobol indices for the Gaussian process metamodel, Reliability Engineering & System Safety, 94, 742–751, 2009.

Mauger, G. S. and Norris, J. R.: Assessing the impact of meteorological history on subtropical cloud fraction, Journal of Climate, 23, 2926–2940, https://doi.org/10.1175/2010JCLI3272.1, 2010.

McGibbon, J. and Bretherton, C. S.: Skill of Ship-Following Large-Eddy Simulations in Reproducing MAGIC Observations across the Northeast Pacific Stratocumulus to Cumulus Transition Region, Journal of Advances in Modeling Earth Systems, 9, 810–831, https://doi.org/10.1002/2017MS000924, 2017.

Mechoso, C. R., Wood, R., Weller, R., Bretherton, C. S., Clarke, A. D., Coe, H., Fairall, C., Farrar, J. T., Feingold, G., Garreaud, R., Grados, C., McWilliams, J., de Szoeke, S. P., Yuter, S. E., and Zuidema, P.: Ocean–Cloud–Atmosphere–Land Interactions in the Southeastern Pacific: The VOCALS Program, Bulletin of the American Meteorological Society, 95, 357 – 375, https://doi.org/10.1175/BAMS-D-11-00246.1, 2014.

Morrison, H. and Milbrandt, J. A.: Parameterization of cloud microphysics based on the prediction of bulk ice particle properties. Part I: Scheme description and idealized tests, Journal of the Atmospheric Sciences, 72, 287–311, 2015.

Nowak, J. L., Dragaud, I. C. D. V., Lee, J., Dziekan, P., Mellado, J. P., and Stevens, B.: A first look at the global climatology of low-level clouds in storm resolving models, Journal of Advances in Modeling Earth Systems, 17, e2024MS004 340, https://doi.org/10.1029/2024MS004340, 2025.

Nugent, J. M., Brown, H., Kirby, A., McCoy, D. T., Allen, G., Aerenson, T., Burrows, S. M., Caulton, D., Fan, J., Feng, Y., Gettelman, A., Griswold, J., Jones, D. B., Leung, L. R., Mahfouz, N., Mikkelsen, A., Mülmenstädt, J., Qian, Y., Shan, Y., Shpund, J., Silber, I., Song, C., Song, X., Wang, H., Wu, M., Xie, S., Zelinka, M. D., Zhang, D., Zhang, G. J., and Zhang, K.: Overview of the Nephele Perturbed Parameter Ensemble for Aerosol-Cloud Interactions in E3SMv3, Journal of Advances in Modeling Earth Systems, 18, e2025MS004 989, https://doi.org/https://doi.org/10.1029/2025MS004989, e2025MS004989 2025MS004989, 2026.

O'Hagan, A.: Bayesian analysis of computer code outputs: A tutorial, Reliability Engineering & System Safety, 91, 1290–1300, https://doi.org/10.1016/j.ress.2005.11.025, 2006.

Peng, L., Blossey, P. N., Hannah, W. M., Bretherton, C. S., Terai, C. R., Jenney, A. M., and Pritchard, M.: Improving Stratocumulus Cloud Amounts in a 200-m Resolution Multi-Scale Modeling Framework Through Tuning of Its Interior Physics, Journal of Advances in Modeling Earth Systems, 16, e2023MS003 632, https://doi.org/https://doi.org/10.1029/2023MS003632, e2023MS003632 2023MS003632, 2024.

Perkins, W. A., Brenowitz, N. D., Bretherton, C. S., and Nugent, J. M.: Emulation of Cloud Microphysics in a Climate Model, Journal of Advances in Modeling Earth Systems, 16, e2023MS003 851, https://doi.org/https://doi.org/10.1029/2023MS003851, e2023MS003851 2023MS003851, 2024.

Prévost, L. M. C., Regayre, L. A., Johnson, J. S., McNeall, D., Milton, S., and Carslaw, K. S.: Detection of potential structural deficiencies in a global aerosol model using a perturbed parameter ensemble, Atmospheric Chemistry and Physics, 26, 2487–2530, https://doi.org/10.5194/acp-26-2487-2026, 2026.

Qu, X., Hall, A., Klein, S. A., and Caldwell, P. M.: On the spread of changes in marine low cloud cover in climate model simulations of the 21st century, Climate dynamics, 42, 2603–2626, 2014.

Rasmussen, C. E. and Williams, C. K. I.: Gaussian Processes for Machine Learning, MIT Press, Cambridge, MA, USA, ISBN 9780262182539, http://www.gaussianprocess.org/gpml/, 2006.

Regayre, L. A., Deaconu, L., Grosvenor, D. P., Sexton, D. M. H., Symonds, C., Langton, T., Watson-Paris, D., Mulcahy, J. P., Pringle, K. J., Richardson, M., Johnson, J. S., Rostron, J. W., Gordon, H., Lister, G., Stier, P., and Carslaw, K. S.: Identifying climate model structural inconsistencies allows for tight constraint of aerosol radiative forcing, Atmospheric Chemistry and Physics, 23, 8749–8768, https://doi.org/10.5194/acp-23-8749-2023, 2023.

https://doi.org/10.5194/egusphere-2026-3700
Preprint. Discussion started: 24 July 2026

Russell, L. M., Lubin, D., Silber, I., Eloranta, E., Muelmenstaedt, J., Burrows, S., Aiken, A., Wang, D., Petters, M., Miller, M., et al.: Eastern Pacific Cloud Aerosol Precipitation Experiment (EPCAPE) Science Plan, Tech. rep., Oak Ridge National Laboratory (ORNL), Oak Ridge, TN (United States). ARM . . . , 2021.

Russell, L. M., Miller, M., Lubin, D., Ackerman, A., Silber, I., Fridlind, A., Eloranta, E., Witte, M., Muelmenstaedt, J., Lebsock, M., Burrows, S., Painemal, D., Aiken, A., Chang, R., Wang, D., Liggio, J., Petters, M., Wheeler, M., et al.: EPCAPE Field Campaign, Final Campaign Report, Tech. Rep. DOE/SC-ARM-25-010, U.S. Department of Energy, 2025.

Saltelli, A., Annoni, P., Azzini, I., Campolongo, F., Ratto, M., and Tarantola, S.: Variance based sensitivity analysis of model output. Design and estimator for the total sensitivity index, Computer Physics Communications, 181, 259–270, https://doi.org/https://doi.org/10.1016/j.cpc.2009.09.018, 2010.

Sanchez, V. A., Carzon, J., Kuusela, M., Gordon, H., and Regayre, L.: Constraining Radiative Impact of Biomass Burning Using Statistical Estimation, in: 106th AMS Annual Meeting, AMS, 2026.

Sandu, I. and Stevens, B.: On the Factors Modulating the Stratocumulus to Cumulus Transitions, Journal of the Atmospheric Sciences, 68, 1865 – 1881, https://doi.org/10.1175/2011JAS3614.1, 2011.

Sansom, R. W. N., Johnson, J. S., Regayre, L. A., Lee, L. A., and Carslaw, K. S.: Strong control of the stratocumulus-to-cumulus transition time by aerosol: analysis of the joint roles of several cloud-controlling factors using Gaussian process emulation, Atmospheric Chemistry and Physics, 26, 1713–1733, https://doi.org/10.5194/acp-26-1713-2026, 2026.

Schneider, T., Teixeira, J., Bretherton, C. S., Brient, F., Pressel, K. G., Schär, C., and Siebesma, A. P.: Climate goals and computing the future of clouds, Nature Climate Change, 7, 3–5, 2017.

Schulte, R. M., Lebsock, M. D., Haynes, J. M., and Hu, Y.: A random forest algorithm for the prediction of cloud liquid water content from combined CloudSat–CALIPSO observations, Atmospheric Measurement Techniques, 17, 3583–3596, 2024.

Schutgens, N., Andrews, E. J., Arola, A., Bhatti, Y., Fu, G., Hasekamp, O., Kolmonen, P., Lipponen, A., Mielonen, T., Reygare, L., and Sayer, A. M.: A satellite-observed climatology of global temporal autocorrelations can be related to aerosol lifetimes, EGUsphere, 2026, 1–30, https://doi.org/10.5194/egusphere-2026-2656, 2026.

Shin, E. Y. and Howland, M. F.: Accelerated Bayesian calibration and uncertainty quantification of RANS turbulence model parameters for stratified atmospheric boundary layer flows, Boundary-Layer Meteorology, 192, 3, 2026.

Silva, S. J., Keller, C. A., and Hardin, J.: Using an explainable machine learning approach to characterize earth system model errors: Application of SHAP analysis to modeling lightning flash occurrence, Journal of Advances in Modeling Earth Systems, 14, e2021MS002 881, 2022.

Sobol, I.: Global sensitivity indices for nonlinear mathematical models and their Monte Carlo estimates, Mathematics and Computers in Simulation, 55, 271–280, https://doi.org/https://doi.org/10.1016/S0378-4754(00)00270-6, the Second IMACS Seminar on Monte Carlo Methods, 2001.

Sobol, I. M.: Sensitivity estimates for nonlinear mathematical models., Math. Model. Comput. Exp., 1, 407–414, 1993.

Stevens, B. and Feingold, G.: Untangling aerosol effects on clouds and precipitation in a buffered system, Nature, 461, 607–613, 2009.

Stevens, B., Feingold, G., Cotton, W. R., and Walko, R. L.: Elements of the microphysical structure of numerically simulated nonprecipitating stratocumulus, Journal of Atmospheric Sciences, 53, 980–1006, 1996.

Stevens, B., Satoh, M., Auger, L., et al.: DYAMOND: the DYnamics of the Atmospheric general circulation Modeled On Non-hydrostatic Domains, Progress in Earth and Planetary Science, 6, 61, https://doi.org/10.1186/s40645-019-0304-z, 2019.

https://doi.org/10.5194/egusphere-2026-3700
Preprint. Discussion started: 24 July 2026

Taylor, M. A., Guba, O., Steyer, A., Ullrich, P. A., Hall, D. M., and Eldred, C.: An energy consistent discretization of the nonhydrostatic equations in primitive variables, Journal of Advances in Modeling Earth Systems, 12, e2019MS001 783, 2020.

Teixeira, J., Cardoso, S., Bonazzola, M., Cole, J., DelGenio, A., DeMott, C., Franklin, C., Hannay, C., Jakob, C., Jiao, Y., Karlsson, J., Kitagawa, H., Köhler, M., Kuwano-Yoshida, A., LeDrian, C., Li, J., Lock, A., Miller, M. J., Marquet, P., Martins, J., Mechoso, C. R., v. Meijgaard, E., Meinke, I., Miranda, P. M. A., Mironov, D., Neggers, R., Pan, H. L., Randall, D. A., Rasch, P. J., Rockel, B., Rossow, W. B., Ritter, B., Siebesma, A. P., Soares, P. M. M., Turk, F. J., Vaillancourt, P. A., Engeln, A. V., and Zhao, M.: Tropical and Subtropical Cloud Transitions in Weather and Climate Prediction Models: The GCSS/WGNE Pacific Cross-Section Intercomparison (GPCI), Journal of Climate, 24, 5223 – 5256, https://doi.org/10.1175/2011JCLI3672.1, 2011.

Terai, C. R., Keen, N. D., Caldwell, P. M., Beydoun, H., Bogenschutz, P. A., Chao, L.-W., Hillman, B. R., Ma, H.-Y., Zelinka, M. D., Bertagna, L., Bradley, A. M., Clevenger, T. C., Donahue, A. S., Foucar, J., Golaz, J.-C., Guba, O., Hannah, W., Lee, J., Lin, W., Mahfouz, N., Mülmenstädt, J., Salinger, A. G., Singh, B., Sreepathi, S., Qin, Y., Taylor, M. A., Ullrich, P. A., Wu, W.-Y., Yuan, X., Zender, C. S., and Zhang, Y.: Radiative, Hydrologic, and Circulation Responses to Warming in Cess-Potter Simulations Using the Global 3.25-km SCREAM, Journal of Advances in Modeling Earth Systems, 17, e2024MS004 930, https://doi.org/https://doi.org/10.1029/2024MS004930, e2024MS004930 2024MS004930, 2025.

Trott, C. R., Lebrun-Grandié, D., Arndt, D., Ciesko, J., Dang, V., Ellingwood, N., Gayatri, R., Harvey, E., Hollman, D. S., Ibanez, D., Liber, N., Madsen, J., Miles, J., Poliakoff, D., Powell, A., Rajamanickam, S., Simberg, M., Sunderland, D., Turcksin, B., and Wilke, J.: Kokkos 3: Programming Model Extensions for the Exascale Era, IEEE Transactions on Parallel and Distributed Systems, 33, 805–817, https://doi.org/10.1109/TPDS.2021.3097283, 2022.

Ukkonen, P.: Exploring pathways to more accurate machine learning emulation of atmospheric radiative transfer, Journal of Advances in Modeling Earth Systems, 14, e2021MS002 875, 2022.

Van der Dussen, J., De Roode, S., Ackerman, A., Blossey, P., Bretherton, C., Kurowski, M., Lock, A., Neggers, R., Sandu, I., and Siebesma, A.: The GASS/EUCLIPSE model intercomparison of the stratocumulus transition as observed during ASTEX: LES results, Journal of Advances in Modeling Earth Systems, 5, 483–499, 2013.

Wong, A. Y. H., Eastham, S. D., Monier, E., and Selin, N. E.: A Geographically Weighted Gaussian Process Regression Emulator of the GCHP 13.0.0 Global Air Quality Model, EGUsphere, 2025, 1–33, https://doi.org/10.5194/egusphere-2025-2663, 2025.

Wood, R.: Stratocumulus Clouds, Monthly Weather Review, 140, 2373–2423, https://doi.org/10.1175/MWR-D-11-00121.1, 2012.

Wood, R., Mechoso, C. R., Bretherton, C. S., Weller, R. A., Huebert, B., Straneo, F., Albrecht, B. A., Coe, H., Allen, G., Vaughan, G., Daum, P., Fairall, C., Chand, D., Gallardo Klenner, L., Garreaud, R., Grados, C., Covert, D. S., Bates, T. S., Krejci, R., Russell, L. M., de Szoeke, S., Brewer, A., Yuter, S. E., Springston, S. R., Chaigneau, A., Toniazzo, T., Minnis, P., Palikonda, R., Abel, S. J., Brown, W. O. J., Williams, S., Fochesatto, J., Brioude, J., and Bower, K. N.: The VAMOS Ocean-Cloud-Atmosphere-Land Study Regional Experiment (VOCALS-REx): goals, platforms, and field operations, Atmospheric Chemistry and Physics, 11, 627–654, https://doi.org/10.5194/acp-11-627-2011, 2011.

Wood, R., O, K.-T., Bretherton, C. S., Mohrmann, J., Albrecht, B. A., Zuidema, P., Ghate, V., Schwartz, C., Eloranta, E., Glienke, S., Shaw, R. A., Fugal, J., and Minnis, P.: Ultraclean Layers and Optically Thin Clouds in the Stratocumulus-to-Cumulus Transition. Part I: Observations, Journal of the Atmospheric Sciences, 75, 1631–1652, https://doi.org/10.1175/JAS-D-17-0213.1, 2018.

Wyant, M. C., Bretherton, C. S., Rand, H. A., and Stevens, D. E.: Numerical Simulations and a Conceptual Model of the Stratocumulus to Trade Cumulus Transition, Journal of the Atmospheric Sciences, 54, 168 – 192, https://doi.org/10.1175/1520-0469(1997)054<0168:NSAACM>2.0.CO;2, 1997.

https://doi.org/10.5194/egusphere-2026-3700
Preprint. Discussion started: 24 July 2026

Xie, S., Terai, C. R., Wang, H., Tang, Q., Fan, J., Burrows, S., Lin, W., Wu, M., Song, X., Zhang, Y., Taylor, M. A., Golaz, J.-C., Benedict, J. J., Chen, C.-C.-J., Feng, Y., Hannah, W. M., Ke, Z., Shan, Y., Larson, V. E., Liu, X., Prather, M. J., Richter, J. H., Shrivastava, M., Wan, H., Zhang, G. J., Zhang, K., Bradley, A. M., Cameron-Smith, P., Damiano, L., Debusschere, B. J., Donahue, A. S., Easter, R. C., Eldred, M. S., Griffin, B. M., Guba, O., Guo, Z., Huang, X., Lee, J., Lee, H.-H., Lou, S., Mahfouz, N., Moncrieff, M., Mülmenstädt, J., Qian, Y., Rasool, Q. Z., Roberts, A. F., Santos, S. P., Sargsyan, K., Shpund, J., Singh, B., Tao, C., Xie, J., Yang, Y., Zeng, X., Zhang, C., Zhang, M., Zhang, S., Zhang, T., Zheng, X., Jacob, R. L., Leung, L. R., McCoy, R. B., and Bader, D. C.: The Energy Exascale Earth System Model Version 3: 1. Overview of the Atmospheric Component, Journal of Advances in Modeling Earth Systems, 17, e2025MS005 120, https://doi.org/https://doi.org/10.1029/2025MS005120, e2025MS005120 2025MS005120, 2025.

Yamaguchi, T., Feingold, G., and Kazil, J.: Stratocumulus to Cumulus Transition by Drizzle, Journal of Advances in Modeling Earth Systems, 9, 2333–2349, https://doi.org/https://doi.org/10.1002/2017MS001104, 2017.

Zhang, H., Zheng, Y., and Li, Z.: Improving Low-Cloud Fraction Prediction Through Machine Learning, Geophysical Research Letters, 51, e2024GL109 735, https://doi.org/https://doi.org/10.1029/2024GL109735, e2024GL109735 2024GL109735, 2024a.

Zhang, H., Zheng, Y., and Li, Z.: Evaluation of stratocumulus evolution under contrasting temperature advections in CESM2 through a Lagrangian framework, Geophysical Research Letters, 51, e2023GL106 856, 2024b.

Zhang, H., Zhang, Y., Li, Z., and Zheng, Y.: Aerosol Influences on Cloud Water: Insights From ARM EPCAPE Observations With Explainable Machine Learning, Geophysical Research Letters, 52, e2025GL115 163, https://doi.org/https://doi.org/10.1029/2025GL115163, e2025GL115163 2025GL115163, 2025.

Zhang, Y., Su, T., Tang, H., Bogenschutz, P., Klein, S. A., Jackson, C., and Caldwell, P.: Process-Oriented Calibration of a Turbulence Scheme in the DOE's Global Storm-Resolving Model Using Machine Learning, Geophysical Research Letters, 53, e2025GL120 241, https://doi.org/https://doi.org/10.1029/2025GL120241, e2025GL120241 2025GL120241, 2026.

Zheng, X., Klein, S. A., Ghate, V. P., Santos, S., McGibbon, J., Caldwell, P., Bogenschutz, P., Lin, W., and Cadeddu, M. P.: Assessment of Precipitating Marine Stratocumulus Clouds in the E3SMv1 Atmosphere Model: A Case Study from the ARM MAGIC Field Campaign, Monthly Weather Review, 148, 3341–3359, https://doi.org/10.1175/MWR-D-19-0349.1, 2020.

Zhou, L., Harris, L., Chen, J.-H., Gao, K., Cheng, K.-Y., Tong, M., et al.: Bridging the gap between global weather prediction and global storm-resolving simulation: Introducing the GFDL 6.5-km SHiELD, Journal of Advances in Modeling Earth Systems, 16, e2024MS004 430, https://doi.org/10.1029/2024MS004430, 2024.

Zhou, X., Kollias, P., and Lewis, E. R.: Clouds, Precipitation, and Marine Boundary Layer Structure during the MAGIC Field Campaign, Journal of Climate, 28, 2420–2442, https://doi.org/10.1175/JCLI-D-14-00320.1, 2015.

Zhu, J., Otto-Bliesner, B. L., Brady, E. C., Eidhammer, T., Gettelman, A., Feng, R., and McCluskey, C. S.: Investigating the State Dependence of Cloud Feedback Using a Suite of Perturbed Parameter Ensembles, Journal of Climate, 38, 4063 – 4081, https://doi.org/10.1175/JCLI-D-24-0686.1, 2025.

Zuidema, P., Chang, P., Medeiros, B., Kirtman, B. P., Mechoso, R., Schneider, E. K., Toniazzo, T., Richter, I., Small, R. J., Bellomo, K., et al.: Challenges and prospects for reducing coupled climate model SST biases in the eastern tropical Atlantic and Pacific oceans: The US CLIVAR Eastern Tropical Oceans Synthesis Working Group, Bulletin of the American Meteorological Society, 97, 2305–2328, 2016.